Experimental Neurology 382 (2024) 114958

Contents lists available at ScienceDirect

Experimental Neurology

journal homepage: www.elsevier.com/locate/yexnr

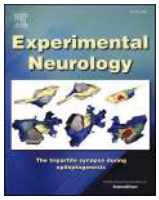

Research paper

Extract from Nasco pomace loaded in nutriosomes exerts anti-inflammatory effects in the MPTP mouse model of Parkinson's disease

Pathik Parekh [a,b], Marcello Serra [a,**], Mohamad Allaw [c], Matteo Perra [c], Annalisa Pinna [d], Maria Manconi [c,*], Micaela Morelli [a,d]

[a] Department of Biomedical Sciences, Section of Neuroscience, University of Cagliari, Cagliari, Italy
[b] Drug Design & Development Section, Translational Gerontology Branch, Intramural Research Program, National Institute on Aging, NIH, Baltimore, MD, USA
[c] Department of Life and Environmental Sciences, University of Cagliari, Italy
[d] National Research Council of Italy, Institute of Neuroscience, Cagliari, Italy

ARTICLE INFO

Keywords:
Astroglia
Microglia
Neuroinflammation
Nanotechnology
Grape pomace extract
Interleukin (IL)-1β
TNF-α

ABSTRACT

Neuroinflammation has recently emerged as a key event in Parkinson's disease (PD) pathophysiology and as a potential target for disease-modifying therapies. Plant-derived extracts, rich in bioactive phytochemicals with antioxidant properties, have shown potential in this regard. Yet their clinical utility is hampered by poor systemic availability and rapid metabolism. Recently, our group demonstrated that intragastric delivery of Nasco pomace extract via nutriosomes (NN), a novel nanoliposome formulation, contrasts the degeneration of nigrostriatal dopaminergic neurons in a subacute 1-methyl-4-phenyl-1,2,3,6-tetrahydropyridine (MPTP) mouse model of PD. In the present study, we investigated the impact of intragastric NN treatment on the reactivity of glial cells in the substantia nigra pars compacta (SNc) and caudate-putamen (CPu) of MPTP-treated mice. To this scope, in mice exposed to MPTP (20 mg/kg/day, × 4 days), we conducted immunohistochemistry analyses of glial fibrillary acidic protein (GFAP) and ionized calcium-binding adapter molecule 1 (IBA1) to assess the responsiveness of astrocytes and microglial cells, respectively. Additionally, we studied the co-localization of the pro-inflammatory interleukin (IL)-1β and tumor necrosis factor (TNF)-α with IBA1 to obtain insights into microglial phenotype. Immunohistochemical results showed that NN administration significantly mitigated astrogliosis and microgliosis in the CPu and SNc of mice receiving subacute MPTP treatment, with region-specific variations in anti-inflammatory efficacy. Remarkably, the CPu showed a heightened response to NN treatment, including a pronounced decrease in microglial IL-1β and TNF-α production. Altogether, these findings underscore the anti-inflammatory effects of NN treatment and provide a potential mechanism underlying the neuroprotective effects previously observed in a subacute MPTP mouse model of PD.

1. Introduction

Parkinson's disease (PD) is the second most prevalent neurodegenerative disorder, impacting approximately 8.5 million individuals worldwide, as indicated by the latest World Health Organization report (2023) (World Health Organization, 2023). Clinically, patients with PD exhibit characteristic motor symptoms, such as tremors, rigidity, bradykinesia, and postural instability, that occur upon the degeneration of 50–70 % of dopaminergic terminals in the caudate-putamen (CPu) (Cheng et al., 2010). These motor disturbances are often preceded or paralleled by one or more non-motor symptoms, exacerbating the overall impact on the patient's quality of life (Obeso et al., 2017). At present, available therapies only alleviate motor and non-motor symptoms associated with PD. However, there is no treatment to cure or slow

Abbreviations: ANOVA, analysis of variance; CPu, caudate-putamen; DAT, dopamine transporter; EN, empty nutriosomes; GFAP, glial fibrillary acidic protein; IBA1, ionized calcium binding adaptor molecule; IL-1β, interleukin-1β; IFN, interferon; i.g, intragastrically; i.p, intraperitoneally; MPTP, 1-methyl-4-phenyl-1,2,3,6-tetrahydropyridine; NN, Nasco nutriosomes; NPE, Nasco pomace extract; PD, Parkinson's disease; ROI, region of interest; SNc, substantia nigra pars compacta; Sal, saline; SNT, simple neurite tracer; TNF, tumor necrosis factor.

* Correspondence to: Dr. Maria Manconi, Department of Life and Environmental Sciences, University of Cagliari, via ospedale,72, Cagliari.
** Correspondence to Dr. Marcello Serra, Department of Biomedical Sciences, Section of Neuroscience, University of Cagliari, Building A, Monserrato University Campus, Monserrato.
E-mail addresses: marcelloserra@unica.it (M. Serra), manconi@unica.it (M. Manconi).

https://doi.org/10.1016/j.expneurol.2024.114958
Received 8 May 2024; Received in revised form 24 August 2024; Accepted 13 September 2024
Available online 18 September 2024

down the progression of the disease (Pardo-Moreno et al., 2023).

In recent years, neuroinflammation has emerged as a central event contributing to PD's pathophysiology and as a potential target for disease-modifying therapies (Jurcau et al., 2023). Neuroinflammation is a complex process primarily orchestrated by two types of glial cells: astrocytes and microglia. Astrocytes, the prevailing glial cell type in the brain, provide structural and metabolic support to surrounding neurons while contributing to the maintenance of the blood-brain barrier integrity (Wang et al., 2023). Microglial cells constitute the principal resident immune cells in the brain and are fundamental in brain development and synaptic plasticity (Andoh and Koyama, 2021). In response to pathogens or brain injuries, astrocytes and microglial cells exhibit heightened proliferation and undergo significant morphological and metabolic changes, adopting a reactive phenotype (gliosis). Depending on the pathological context and the duration of glial activation, this reactive state can yield either beneficial or deleterious effects on neighboring neurons (Gelders et al., 2018). Previous neuroimaging and *post-mortem* investigations conducted on experimental models of PD and patients with PD have provided evidence of widespread gliosis affecting several brain regions, including the substantia nigra pars compacta (SNc), CPu, thalamus, and cortex (Cebrián et al., 2014; McGeer et al., 1988; Ouchi et al., 2005). Importantly, reactive glial cells predominantly express a pro-inflammatory phenotype, characterized by the production of inflammatory mediators, including reactive oxygen species, chemokines, and cytokines, such as tumor necrosis factor (TNF)-α, interferon (IFN)-γ, interleukin (IL)-1β, IL-6, and IL-2 (Liu et al., 2022; Tansey et al., 2022). Over time, the persistence of this proinflammatory environment significantly compromises the viability of nigrostriatal dopaminergic neurons.

Plant-based extracts have received great interest owing to their favorable tolerability and abundance in biologically active phytochemicals that can potentially modulate immune responses through multifaceted mechanisms (Parkhe et al., 2020; Parekh et al., 2022Parekh et al., 2022; Yin et al., 2021). Due to their physicochemical properties (e.g. hydrophobicity, low aqueous solubility, and large size), low gastrointestinal absorption, and rapid metabolism, these natural compounds are often encapsulated within nanovesicle systems before their utilization. Compared with standard solutions containing the free form of a drug, this pharmacological strategy was found effective in improving the solubility, stability, and bioavailability of these phytochemicals, especially when administrated orally (Manconi et al., 2020; Roy et al., 2023). Among the available nanovesicle systems, liposomes, namely nano-sized spherical vesicles composed of an aqueous core surrounded by one or more lipid bilayers, have attracted much attention in the pharmacognosy and nutraceutical fields due to their high biocompatibility, flexible physicochemical and biophysical properties, and ease of preparation. Moreover, their ability to encapsulate both hydrophobic and hydrophilic compounds has been shown to be particularly effective in enhancing their value as drug-delivery systems (Lombardo and Kiselev, 2022).

Starting from this compelling evidence, we recently assessed the neuroprotective effects of the grape pomace extract from the Nasco *Vitis vinifera* (NPE) in the subacute 1-methyl-4-phenyl-1,2,3,6-tetrahydropyridine (MPTP) mouse model of PD (Parekh et al., 2022), wherein the degeneration of dopaminergic nigrostriatal neurons, while significant, does not manifest overt motor deficits (Pupyshev et al., 2019; Santoro et al., 2023). NPE (100 mg/kg) was administrated intragastrically (i.g.) either as a free suspension or following encapsulation in nano-liposomes formed by the combination of maltodextrin Nutriose® FM06 and the phospholipid S75 (Allaw et al., 2020), referred to as nutriosomes. Significantly, our investigation demonstrated that the administration of NPE through nutriosomes (NN), but not the suspension, conferred notable protection to tyrosine hydroxylase (TH)-positive neurons and fibers comprising the nigrostriatal tract against the subacute neurotoxic effects of MPTP (Parekh et al., 2022). Nonetheless, the precise mechanisms underpinning the neuroprotective effects of NN treatment remained unexplored.

Given the enrichment of NPE with antioxidant polyphenols (e.g., gallic acid, catechin, epicatechin, procyanidin B2, and quercetin) and the pronounced gliosis observed in the brain of mice subjected to subacute MPTP treatment (20 mg/kg/day, 4-consecutive days, intraperitoneally (i.p.)) (Costa et al., 2013; Frau et al., 2011), in the present study we aim to address, through immunohistochemical evaluations, the impact and temporal dynamics of NN treatment in the counteraction of neuroinflammatory events occurring in the CPu and SNc of MPTP-treated mice.

2. Materials and methods

2.1. Chemicals and drugs

MPTP-HCl was purchased from MedChem Express, USA (HY-15608) and dissolved in distilled water. Grape pomaces, generated from the vinification process of the Nasco variety of *Vitis vinifera,* were provided by a local winery (Cantine Argiolas), and were harvested in southern Sardinia (Italy) in September–October 2020. Samples were dried and stored under vacuum at −20 °C until use. Lipoid S75 was purchased from Lipoid (Ludwigshafen, Germany). Nutriose® FM06 was donated by Roquette (Lestrem Cedex, France). Ethanol and all other products were of analytical grade and were purchased from Merck (Milan, Italy).

2.2. Animals

Fifty-three 16–19 weeks old male C57BL/6 J mice (Charles River, Calco, Italy) weighing 25 ± 2 g at the beginning of the experiments were used. Mice were housed in a group of 4 per cage under constant temperature and a 12-h light/dark cycle. Standard laboratory chow and tap water were available ad libitum. All experiments were conducted in adherence with the guidelines for animal experimentation of the EU directives (2010/63/EU; L.276; 22/09/2010) and with the guidelines issued by the Organism for Animal Welfare (OPBA) of the University of Cagliari. Experiments were designed to minimize animal discomfort and to reduce the number of animals used.

2.3. Experimental plan

Fig. 1 illustrates the experimental plan. Fifty-three mice were randomly allocated into four experimental groups based on the respective treatments: 1) saline (SAL) + vehicle (VEH), $n = 11$; 2) Nasco nutriosomes (NN) (100 mg/kg) + VEH, $n = 5$; 3) Empty nutriosomes (EN) + MPTP (20 mg/kg): $n = 16$; 4) Nasco nutriosomes (NN) (100 mg/kg) + MPTP (20 mg/kg), $n = 21$. SAL, EN, and NN were administered i.g. via gavage (18-gauge) in a volume of 10 mL/kg of body weight. VEH and MPTP (20 mg/kg/day x 4 consecutive days) were given i.p. in a volume of 10 mL/kg of body weight. Before treatment, mice underwent one week of handling by experimenters (two daily sessions, 5 min each) to reduce animal distress. On day 1 (pre-treatment), mice received either SAL, EN, or NN. From day 2 to day 5 (combined treatment), mice received a daily i.p. injection of either VEH or MPTP. MPTP treatment was preceded (3 h prior) and succeeded (4 h later) by an i.g. administration of either SAL, EN, or NN. Thereafter, mice were divided into two groups for post-treatment in order to receive either a single i.g. administration (on day 6) or three consecutive i.g. administrations (from day 6 to day 8, once per day) of either SAL, EN, or NN. The dosage, route, and administration schedule of NN were determined according to a prior investigation by our group (Parekh et al., 2022).

2.4. Immunohistochemical experiments

2.4.1. Tissue preparation

Thirty minutes after the last i.g. administration of SAL, EN, or NN (on days 6 and 8), mice were deeply anaesthetized and transcardially

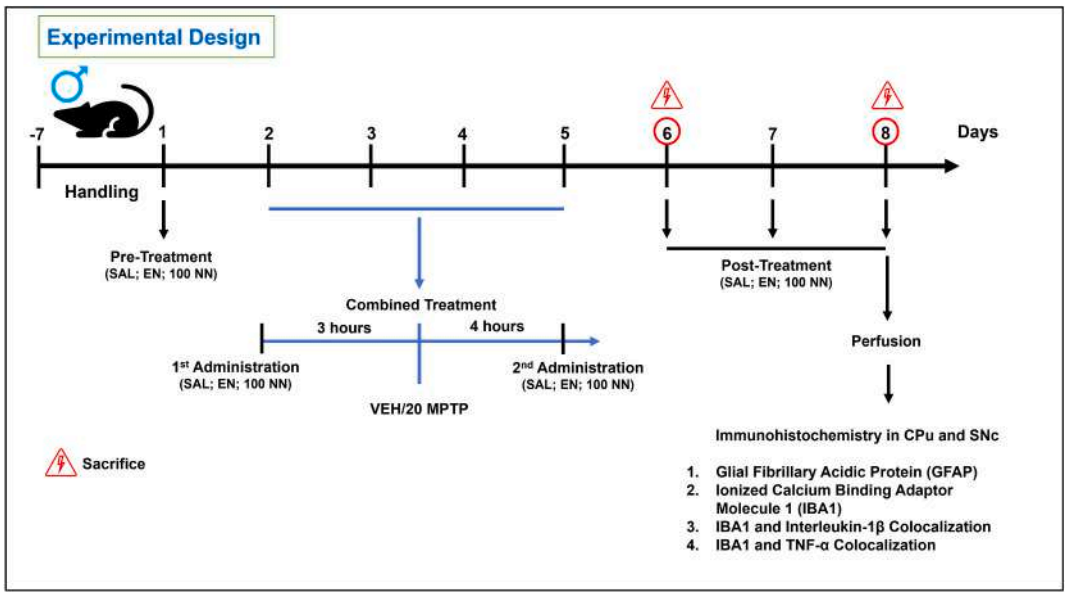

Fig. 1. Illustration of the experimental design. CPu: caudate-Putamen nucleus; EN: empty nutriosomes; MPTP: 1-methyl-4-phenyl-1,2,3,6-tetrahydropyridine; NN: Nasco nutriosomes; SAL: saline; SNc: substantia nigra pars compacta; VEH: distilled water; TNF-α: tumor necrosis factor-α. Numbers indicate the dose of each compound, expressed in mg/kg.

perfused with ice-cold saline (NaCl, 0.9 % *w/v*) followed by 4 % paraformaldehyde (PFA) in 0.1 M phosphate buffer (PB, pH 7.4). Subsequently, their brains were isolated, post-fixed in 4 % PFA for 2 h, and preserved in PB saline 1× (PBS) at 4 °C. On the subsequent day, brains were coronally cut on a vibratome (VT1000S, Leica Biosystems) to yield sections (50 μm thick) suited for immunohistochemical processing.

For each mouse, three coronal sections were obtained according to the following stereotaxic coordinates: A) CPu: 1.34 to 0.74 mm, B) SNc: −2.92 to −3.52 mm relative to bregma, according to the mouse brain atlas (Franklin and Paxinos, 2008).

2.4.2. Immunofluorescence for glial fibrillary acidic protein (GFAP), ionized calcium binding adaptor molecule 1 (IBA1), dopamine transporter (DAT), interleukin-1β (IL-1β), and tumor necrosis factor alpha (TNF-α)

Immunohistochemical evaluation of GFAP, IBA1, IL-1β, TNF-α, and DAT was carried out as previously described (Pinna et al., 2021). In brief, free-floating sections were rinsed in 0.1 M PB, blocked, and permeabilized in 0.1 M PB containing 3 % normal goat serum/ normal donkey serum, 0.05 % bovine serum albumin (BSA) and 0.3 % Triton X-100 at room temperature (3 h), followed by incubation in the same solution with one or a combination of the following primary antibodies: mouse anti-GFAP (1:1000; Merck, Italy, G3893) either alone (for CPu) or plus rat anti-DAT (1:1000, Millipore, USA, MAB369) (for SNc), rabbit anti-IBA1 (1:600, Wako, USA, 019–19741) plus Armenian hamster anti-IL-1β (1:50, Santa Cruz Biotechnology, USA, sc-12,742) or mouse anti-TNF-α (1:50, Santa Cruz Biotechnology, USA, sc-133192). Incubation with primary antibodies was performed at 4 °C for 1 night. Then, sections were incubated at room temperature with the appropriate secondary antibodies, as follows: 1) for GFAP, AlexaFluor®488-labeled donkey anti-mouse (1:500, Jackson ImmunoResearch, UK, 715–547-003) (1 h); 2) for DAT, biotinylated goat anti-rat (1:200, Vector lab, USA, BA-9401) (2 h) followed by AlexaFluor®594-labeled streptavidin (1:500, Jackson ImmunoResearch, UK, 016–580-084) (1 h); 3) for IBA1, AlexaFluor®594-labeled goat anti-rabbit (1200, Jackson ImmunoResearch, UK, 111–585-003) (2 h); 4) for IL-1β, AlexaFluor®488-labeled goat anti-hamster (1200, Invitrogen, USA, A21110) (2 h); 5) for TNF-α, AlexaFluor®488-labeled goat anti-mouse (1200, Jackson ImmunoResearch, UK, 115–545-008) (3 h). Afterward, sections were incubated for 10 min in 4′,6-diamidino-2-phenylindole (DAPI; 1:10,000, Merck, Italy, D9542), to allow visualization of cell nuclei, rinsed in PB 0.1, and mounted onto super-frost glass slides using Mowiol® mounting medium. Omission of either the primary or secondary antibodies served as negative control and yielded no labeling (data not shown).

2.4.3. Image acquisition and analysis

Images of a single wavelength (14-bit depth) were obtained with the ZEISS Axio Scan Z1 slide scanner (Zeiss, Germany) as previously described (Serra et al., 2023). Brain sections immunostained for GFAP, DAT, and IBA1 were captured at 20× magnification (Objective: Plan-Apochromat 20×/0.8 M27) to acquire the two portions from the CPu (dorsolateral and dorsomedial) and the whole SNc, left and right hemispheres. The ImageJ software (National Institutes of Health, USA) was used to quantify: (1) the total number of GFAP-positive cells in the CPu and SNc, (2) the total number of IBA1-positive cells in the CPu and SNc. To quantify GFAP-positive cells in the CPu and SNc and IBA1-positive cells in the CPu, images were first converted to 8-bit, background adjusted, then cells were manually counted in fixed regions by using the multi-point tool. For the GFAP-positive cells in the SNc, the region of interest (ROI) was first identified by checking the presence of dopaminergic neurons immunoreactive for DAT. To quantify IBA1-positive cells in the SNc, the images were converted to 8-bit and background adjusted. Thereafter, the cells were counted by using the multi-point tool across the whole SNc. Analyses were performed in a blinded manner in the three sections. No significant differences in the number of GFAP- and IBA1-positive cells were found among the three sections and two ROIs within the CPu (dorsolateral and dorsomedial). Thus, values from different levels and ROIs were averaged, normalized with respect to the SAL/VEH group, and expressed as a percentage.

2.4.4. Morphometric analysis of GFAP-positive cells in the caudate-putamen (CPu) and substantia nigra pars compacta (SNc)

For the morphometric analysis of GFAP-positive cells in the CPu and SNc, confocal images of a single wavelength (16-bit depth) from the dorsolateral and dorsomedial CPu, and the whole SNc, left and right hemispheres, were digitalized and captured by using a motorized (Mad City Labs MCL MOTZN) inverted epifluorescence microscope (Zeiss Axio Observer A1; objective: Plan-Apochromat 63×/1,40, OIL M27) equipped with the CREST CARVII spinning disk system and connected to the Prime BSI sCMOS digital camera (4.2 Megapixels; Teledyne photometrics, US). Tridimensional (3D) reconstruction of the astrocytic backbone

was conducted semi-automatically utilizing the Simple Neurite Tracer (SNT) plug-in on the open-source software ImageJ, as previously described (Bondi et al., 2021; Tavares et al., 2017). This analysis provides multiple characteristics of the astrocytic structure, such as total process length, number of processes, and the total number of process intersections given by the maximum intersection radius (Sholl analysis). In detail, 3D reconstruction was carried out on z-stack confocal images (z-stack = 25 μm; z-stack interval: 0.5 μm) and involved exclusively GFAP-immunoreactive astrocytes (n = 15–16 astrocytes per animal) having fully preserved processes along the x-y-z axis and a clear DAPI-stained nucleus. DAPI-positive nuclei were used to define the astrocyte centre, around which every primary process originates. Next, a distant point within the primary process was selected, and SNT automatically determined the process midline and tortuosity. After confirming the automatically detected path, this step was repeated until the primary process, respective branches, and branchlets were reconstructed entirely. For the systematic categorization of astrocytic processes into secondary, tertiary, and quaternary levels, we employed a structured approach. Processes branching directly off the primary process were classified as secondary. Tertiary processes were those emanating from the secondary branches, while quaternary processes arose from the tertiary branches. This hierarchical segmentation was pivotal for our in-depth morphometric analysis. Thereafter, we performed the morphometric analysis on 3D reconstructed astrocytes by using the Sholl analysis plugin (Ferreira et al., 2014), using the following settings (enclosing radius cutoff = 1 intersection, Sholl method = linear) with radii increasing by 5 μm. The Sholl intersection profile counts the number of intersections between the astrocytic process and concentric spheres emanating from the centre of cell soma. Reconstructed astrocytes in Fig. 4 were selected to represent the total process length, number of processes, and number of intersections closest to the group mean.

2.4.5. Colocalization analysis between IBA1 and either IL-1β or TNF-α in the caudate-putamen (CPu) and substantia nigra pars compacta (SNc)

For colocalization analysis between IL-1β/IBA1 and TNF-α/IBA1, confocal images of a single wavelength (16-bit depth) from the dorsolateral and dorsomedial CPu and the whole SNc, left and right hemispheres, were acquired at 63× (for IL-1β/IBA1) and 100× (for TNF-α/IBA1) as described previously (**see** Section 2.4.4).

The colocalization analysis was conducted using the ImageJ plug-in JACoP (Just Another Colocalization Plugin) (Bolte and Cordelières, 2006). Approximately 25–30 IBA1-positive cells were randomly selected within the CPu and SNc of each mouse for the colocalization analysis. Specifically, two regions of interest (ROIs) were identified for both the CPu (dorsolateral and dorsomedial) and the SNc (dorsolateral and ventromedial). Thereafter, we measured the correlation of signal intensity between IBA1 and IL-1β or TNF-α immunostaining through Mander's correlation coefficient (R). This coefficient serves as a semi-quantitative measure to estimate the extent of overlap between two distinct fluorescence signals (Dunn et al., 2011). Analyses were performed in a blinded manner in the three sections. No significant differences in the correlation coefficient were found among the three sections and two ROIs within the given area. Thus, values from different levels and ROIs were averaged, normalized with respect to the SAL/VEH group, and expressed as a percentage.

2.5. Data analysis and statistics

Statistical analysis was carried out with GraphPad Prism 8 software (GraphPad Software, Inc., La Jolla, CA), and, for each time point (1 day and 3 days), data were analyzed by two-way analysis of variance (ANOVA; pre-treatment × pre-treatment) followed by Tukey's post hoc test. Results are expressed as mean ± SEM and were considered statistically significant if $p < 0.05$.

3. Results

3.1. Immunoreactivity of GFAP in the caudate-putamen (CPu) following subacute MPTP and Nasco nutriosome treatment

Subacute MPTP treatment significantly increased the number of GFAP-positive cells in the dorsal CPu of the mice sacrificed either 1 day (~1330 %) or 3 days (~1350 %) following the last MPTP administration (Fig. 2A-C). Administration of NN (100 mg/kg) attenuated the MPTP-induced increase in GFAP-positive cell numbers, irrespective of the time of sacrifice (Fig. 2A, B).

Two-way ANOVA revealed significant effects of NN treatment (1 day: $F_{1,31} = 12$, $p = 0.0016$; 3 days: $F_{1,30} = 15.75$, $p = 0.0004$), MPTP treatment (1 day: $F_{1,31} = 1825$, $p < 0.0001$; 3 days: $F_{1,30} = 1055$, $p < 0.0001$), and NN treatment × MPTP treatment interaction (1 day: $F_{1,31} = 12.01$, $p = 0.0016$; 3 days: $F_{1,30} = 15.75$, $p = 0.0004$). Tukey's post hoc test indicated a significant increase in the number of GFAP-positive cells in mice receiving MPTP in combination with either EN or NN compared with both SAL/VEH- and NN/VEH-treated mice. This effect was evident at both the 1-day ($p < 0.0001$) and 3-day ($p < 0.0001$) time points (Fig. 2A, B). Irrespective of the sacrifice time, NN/MPTP treatment significantly reduced the total number of GFAP-positive cells compared with EN/MPTP ($p < 0.01$) (Fig. 2A, B). The results obtained are summarized in Table 1.

3.2. Immunoreactivity of GFAP in the substantia nigra pars compacta (SNc) following subacute MPTP and Nasco nutriosome treatment

Subacute MPTP treatment increased the number of GFAP-positive cells in the SNc of the mice sacrificed either 1 day (~40 %) or 3 days (~70 %) from the last MPTP administration (Fig. 3A-C**)**. Administration of NN (100 mg/kg) significantly mitigated the MPTP-induced increase in GFAP-positive cell numbers in mice sacrificed 3 days, but not 1 day, after MPTP treatment (Fig. 3A-C).

At 1 day after MPTP treatment, two-way ANOVA revealed a significant effect of MPTP treatment ($F_{1,31} = 30.26$, $p < 0.0001$). Tukey's post hoc test indicated a significant increase in the number of GFAP-positive cells in mice receiving EN/MPTP compared with both SAL/VEH- ($p < 0.001$) and NN/VEH-treated mice ($p < 0.05$), and NN/MPTP compared with SAL/VEH ($p < 0.001$) (Fig. 3A-C).

At 3 days after MPTP treatment, two-way ANOVA revealed significant effects of NN treatment ($F_{1,30} = 4.970$, $p = 0.0334$), MPTP treatment ($F_{1,30} = 52.39$, $p < 0.0001$), and NN treatment × MPTP treatment interaction ($F_{1,30} = 17.90$, $p = 0.0002$). Tukey's post hoc test indicated a significant increase in the number of GFAP-positive cells in mice receiving EN/MPTP compared with both SAL/VEH- ($p < 0.0001$) and NN/VEH-treated mice ($p < 0.0001$), and NN/MPTP compared with SAL/VEH ($p < 0.01$) (Fig. 3A-C). Remarkably, at this time point, NN/MPTP treatment significantly reduced the number of GFAP-positive cells compared with EN/MPTP ($p < 0.0001$) (Fig. 3A-C). The results obtained are summarized in Table 1.

3.3. Morphometric analysis of GFAP-positive astrocytes in the caudate-putamen (CPu) and substantia nigra pars compacta (SNc) following subacute MPTP and Nasco nutriosomes treatment

Subacute MPTP treatment significantly altered the morphological characteristics (e.g. number of processes, total length, and number of intersections) of GFAP-positive cells in the dorsal CPu and SNc of mice sacrificed after either 1 day or 3 days following the last MPTP administration (Fig. 4A-H). Conversely, NN treatment did not elicit any effects on astrocyte morphology.

In the CPu, two-way ANOVA revealed a significant effect of MPTP treatment on the number of processes (1 day: $F_{1,19} = 92.26$, $p < 0.0001$; 3 days: $F_{1,19} = 144.9$, $p < 0.0001$), total length (1 day: $F_{1,19} = 61.09$, $p < 0.001$; 3 days: $F_{1,19} = 218.0$, $p < 0.0001$), and number of intersections

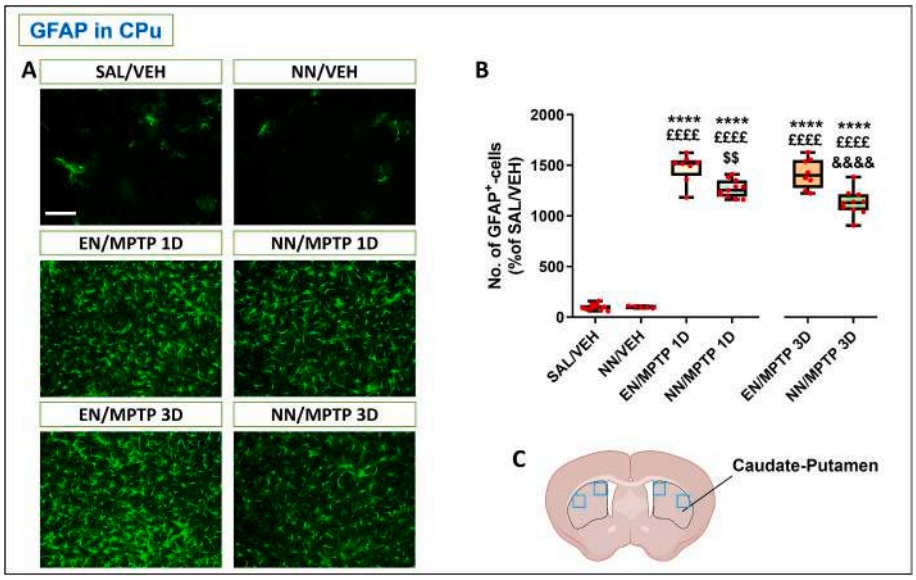

Fig. 2. Effect of NN (100 mg/kg) on the immunoreactivity of glial fibrillary acidic protein (GFAP) in the caudate-putamen (CPu) of MPTP-treated mice. (A) Representative images of dorsomedial CPu immunostained for GFAP. (B) Total number of GFAP-positive cells in the CPu of mice sacrificed either 1 day or 3 days following the last MPTP administration. (C) Areas of CPu (blue squares) used for quantitative analysis. Values are expressed as a percentage of the SAL/VEH group. Red dots within boxes represent individual mice. Box plots indicate the top and bottom quartiles; whiskers refer to top and bottom 90 %. ****$p < 0.0001$ vs. SAL/VEH; $^{\text{£££}}p < 0.0001$ vs. NN/VEH; $^{\$\$}p < 0.01$ vs. EN/MPTP 1D; $^{\&\&\&\&}p < 0.0001$ vs. EN/MPTP 3D. Scale bar = 50 μm. D: day(s); EN: empty nutriosomes; MPTP: 1-methyl-4-phenyl-1,2,3,6-tetrahydropyridine; NN: Nasco nutriosomes; SAL: saline; VEH: vehicle (distilled water). SAL/VEH: $n = 11$; NN/VEH: $n = 5$; EN/MPTP: 1D $n = 8$; NN/MPTP 1D: n = 11; EN/MPTP 3D: n = 8; NN/MPTP 3D: $n = 10$. (For interpretation of the references to colour in this figure legend, the reader is referred to the web version of this article.)

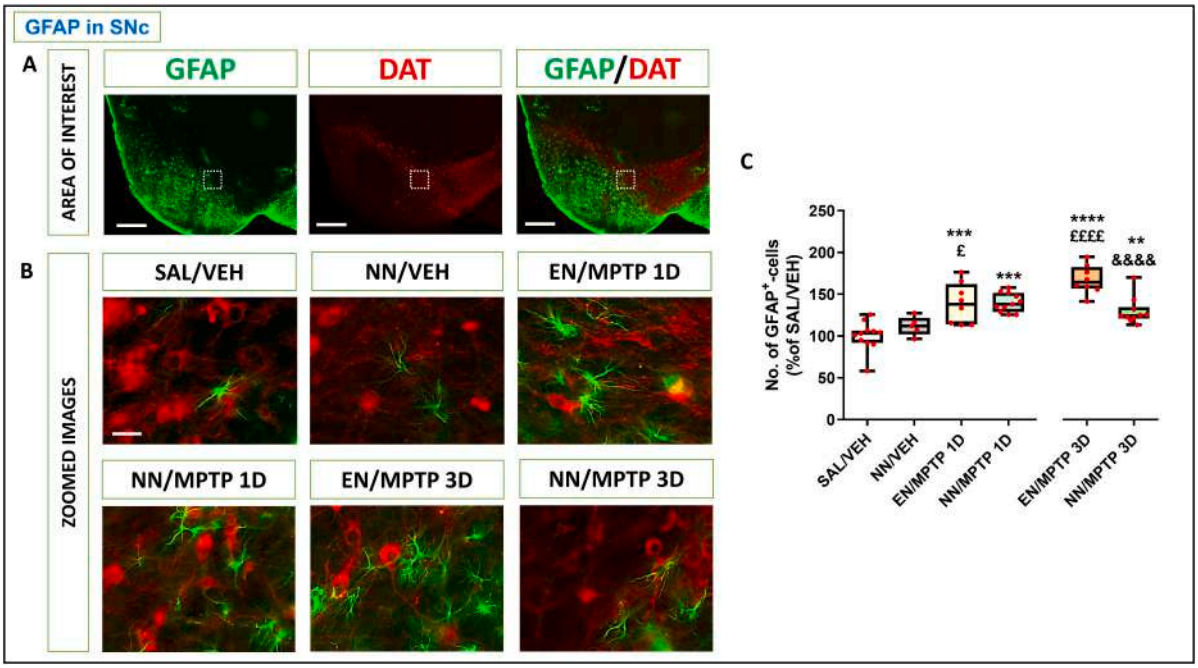

Fig. 3. Effect of NN (100 mg/kg) on the immunoreactivity of glial fibrillary acidic protein (GFAP) in the substantia nigra pars compacta (SNc) of MPTP-treated mice. (A-B) Representative sections of the SNc immunostained for GFAP and dopamine transporter (DAT), and the areas of the SNc used for the quantitative analysis. (C) Total number of GFAP-positive cells in the SNc of mice sacrificed either 1 day or 3 days following the last MPTP administration. Values are expressed as a percentage of the SAL/VEH group. Red dots within boxes represent individual mice. Box plots indicate the top and bottom quartiles; whiskers refer to top and bottom 90 %. **$p < 0.01$, ***$p < 0.001$, ****$p < 0.0001$ vs. SAL/VEH; $^{£}p < 0.05$, $^{\text{£££}}p < 0.0001$ vs. NN/VEH; $^{\&\&\&\&}p < 0.0001$ vs. EN/MPTP 3D. Scale bar = 500 μm (20×), 10 μm (zoom). D: day(s); EN: empty nutriosomes; MPTP: 1-methyl-4-phenyl-1,2,3,6-tetrahydropyridine; NN: Nasco nutriosomes; SAL: saline; VEH: vehicle (distilled water). SAL/VEH: $n = 11$; NN/VEH: $n = 5$; EN/MPTP: 1D $n = 8$; NN/MPTP 1D: n = 11; EN/MPTP 3D: n = 8; NN/MPTP 3D: $n = 10$. (For interpretation of the references to colour in this figure legend, the reader is referred to the web version of this article.)

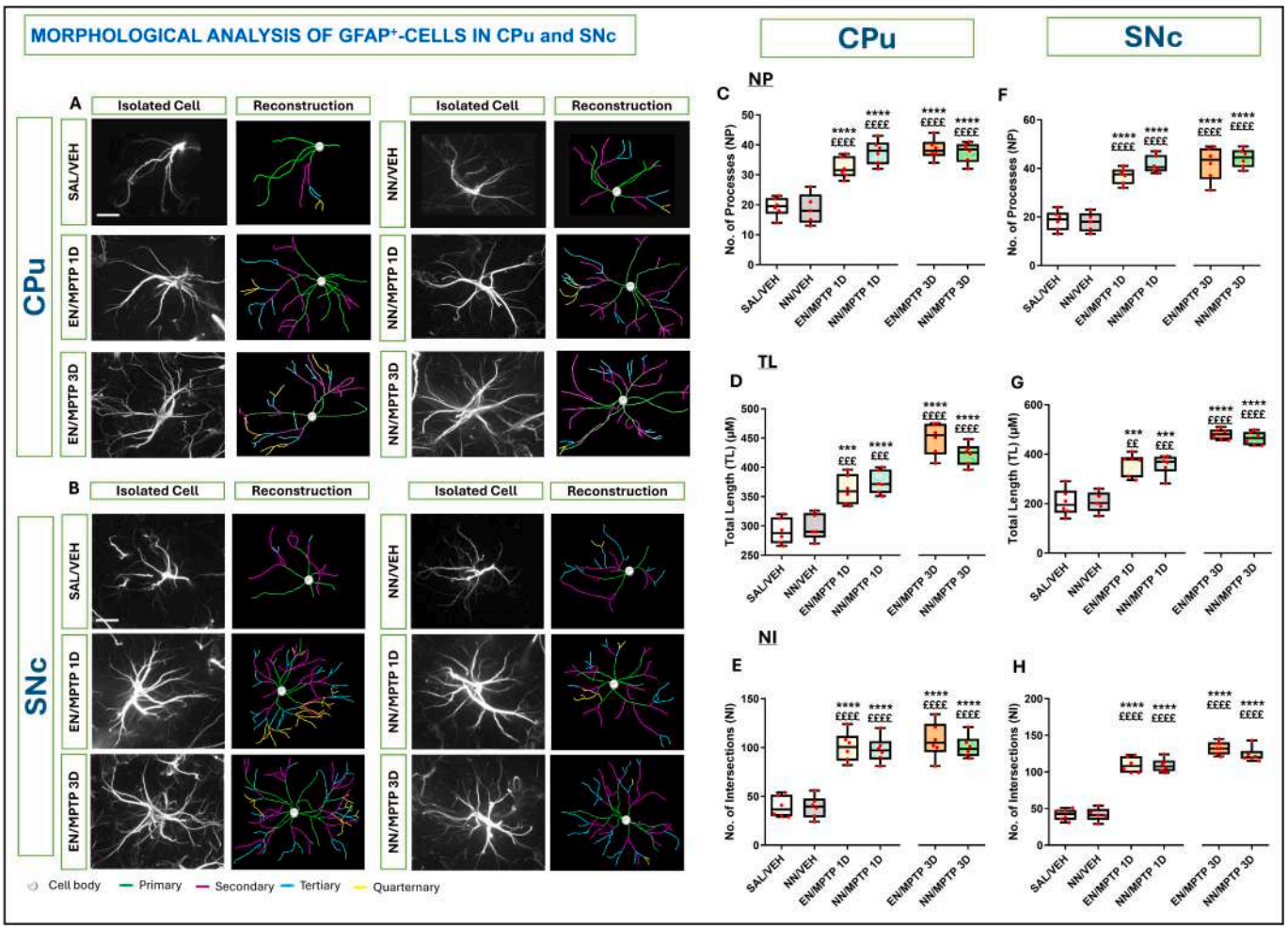

Fig. 4. Effect of NN (100 mg/kg) on the morphological characteristics of glial fibrillary acidic protein (GFAP)-positive cells in the caudate-putamen (CPu) and substantia nigra pars compacta (SNc) of MPTP-treated mice. (A-B) Representative confocal images and related 3D reconstruction of isolated GFAP-positive cells in the (A) dorsomedial CPu and (B) SNc. (C) The number of processes (NP), (D) the total length (TL), and (E) the number of intersections (NI) of isolated GFAP-positive cells (n = 18–20 cells/mouse) in the CPu of mice sacrificed either 1 day or 3 days following the last MPTP administration. (F) The number of processes, (G) the total length, and (H) the number of intersections of isolated GFAP-positive cells (n = 18–20 cells/mouse) in the SNc of mice sacrificed either 1 day or 3 days following the last MPTP administration. Red dots within boxes indicate the values of individual mice. Box plots indicate the top and bottom quartiles; whiskers refer to top and bottom 90 %. ***$p < 0.001$, ****$p < 0.0001$ vs. SAL/VEH; $^{££}p < 0.01$, $^{£££}p < 0.001$, $^{££££}p < 0.0001$ vs. NN/VEH; Two-way ANOVA followed by Tukey's post hoc test. Scale bar = 10 µm. D: day(s); EN: empty nutriosomes; MPTP: 1-methyl-4-phenyl-1,2,3,6-tetrahydropyridine; NN: Nasco nutriosomes; SAL: saline; VEH: vehicle (distilled water). SAL/VEH: n = 6; NN/VEH: n = 5; EN/MPTP: 1D n = 6; NN/MPTP 1D: n = 6; EN/MPTP 3D: n = 6; NN/MPTP 3D: n = 6. (For interpretation of the references to colour in this figure legend, the reader is referred to the web version of this article.)

(1 day: $F_{1,19} = 121.0$, $p < 0.0001$; 3 days: $F_{1,19} = 128.9$, $p < 0.0001$) at both time points. Tukey's post hoc test indicated a significant increase in the number of processes, total length, and number of intersections of 3D-reconstructed GFAP-positive cells of mice receiving MPTP in combination with either EN or NN compared with both SAL/VEH- and NN/VEH-treated mice. This effect was evident at both the 1-day ($p < 0.001$) and 3-day ($p < 0.0001$) time points (Fig. 4A, C-E).

In the SNc, two-way ANOVA revealed a significant effect of MPTP treatment on the number of processes (1 day: $F_{1,19} = 94.79$, $p < 0.0001$; 3 days: $F_{1,19} = 127.0$, $p < 0.0001$), total length (1 day: $F_{1,19} = 50.48$, $p < 0.001$; 3 days: $F_{1,19} = 154.2$, $p < 0.0001$), and number of intersections (1 day: $F_{1,19} = 188.0$, $p < 0.0001$; 3 days: $F_{1,19} = 247.5$, $p < 0.0001$) at both time points. Tukey's post hoc test indicated a significant increase in the number of processes, total length, and number of intersections of 3D-reconstructed GFAP-positive cells of mice receiving MPTP in combination with either EN or NN compared with both SAL/VEH- and NN/VEH-treated mice. This effect was evident at both the 1-day ($p < 0.01$) and 3-day ($p < 0.0001$) time points (Fig. 4B, F-H).

3.4. Immunoreactivity of IBA1 in the caudate-putamen (CPu) following subacute MPTP and Nasco nutriosomes treatment

Subacute MPTP treatment significantly increased the number of IBA1-positive cells in the dorsal CPu of mice sacrificed after either 1 day (number: ~31 %) or 3 days (number: ~23 %) following the last MPTP administration (Fig. 5A-C). Administration of NN (100 mg/kg) significantly contrasted the MPTP-induced elevation in IBA1 immunoreactivity in mice sacrificed 3 days, but not 1 day, after MPTP treatment (Fig. 5A, B).

At 1 day after MPTP treatment, two-way ANOVA revealed a significant effect of MPTP treatment on the number of IBA1-positive cells ($F_{1,31} = 40.44$, $p < 0.0001$). Tukey's post hoc test indicated a significant increase in the number of IBA1-positive cells in mice receiving MPTP in combination with either EN or NN compared with both SAL/VEH- ($p < 0.01$) and NN/VEH-treated mice ($p < 0.01$) (Fig. 5A, B).

At 3 days after MPTP treatment, two-way ANOVA revealed significant effects of NN treatment ($F_{1,30} = 11.18$, $p = 0.0022$), MPTP treatment ($F_{1,30} = 16.64$, $p = 0.0003$), and NN treatment × MPTP treatment

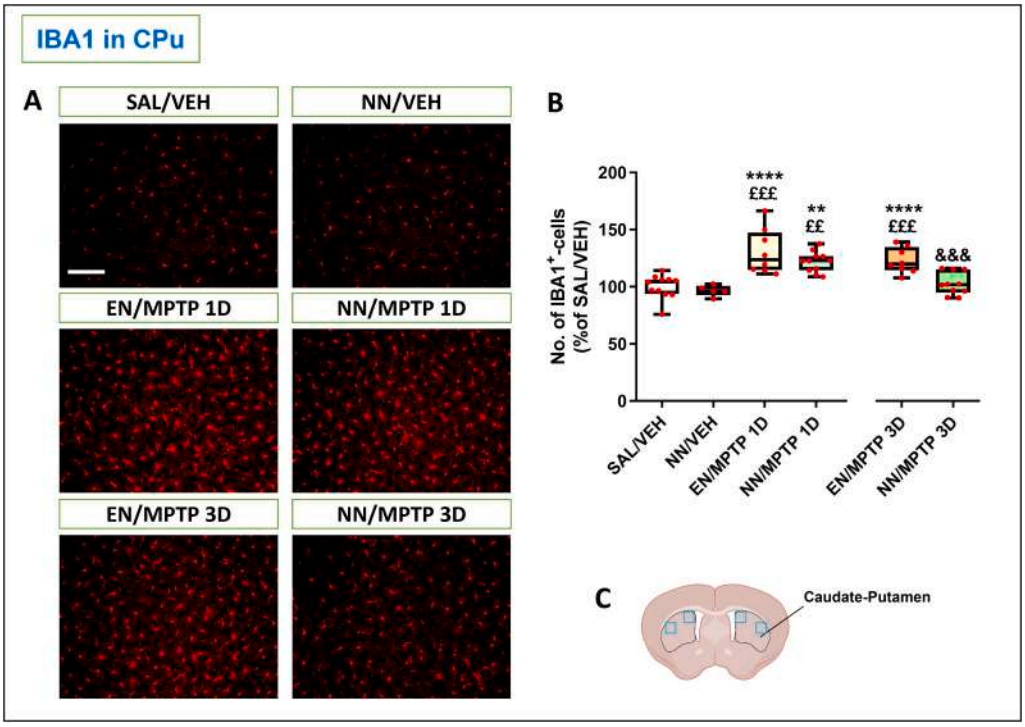

Fig. 5. Effect of NN (100 mg/kg) on the immunoreactivity of ionized calcium-binding adaptor molecule 1 (IBA1) in the caudate-putamen (CPu) of MPTP-treated mice. (A) Representative sections of the dorsomedial CPu immunostained for IBA1. (B) Total number of IBA1-positive cells in the CPu of mice sacrificed either 1 day or 3 days following the last MPTP administration. (C) Areas of the CPu (blue squares) used for the quantitative analysis. Values are expressed as a percentage of the SAL/VEH group. Red dots within boxes indicate the values of individual mice. Box plots indicate the top and bottom quartiles; whiskers refer to top and bottom 90 %. $^{**}p < 0.01$, $^{****}p < 0.0001$ vs. SAL/VEH; $^{££}p < 0.01$, $^{£££}p < 0.001$ vs. NN/VEH; $^{\&\&\&}p < 0.001$ vs. EN/MPTP 3D. Scale bar = 50 μm. D: day(s); EN: empty nutriosomes; MPTP: 1-methyl-4-phenyl-1,2,3,6-tetrahydropyridine; NN: Nasco nutriosomes; SAL: saline; VEH: vehicle (distilled water). SAL/VEH: $n = 11$; NN/VEH: $n = 5$; EN/MPTP: 1D $n = 8$; NN/MPTP 1D: n = 11; EN/MPTP 3D: n = 8; NN/MPTP 3D: $n = 10$. (For interpretation of the references to colour in this figure legend, the reader is referred to the web version of this article.)

interaction ($F_{1,30} = 5.423$, $p = 0.0268$) on the total number of IBA1-positive cells. Tukey's post hoc test indicated a significant increase in the number of IBA1-positive cells in mice receiving EN/MPTP compared with both SAL/VEH- ($p < 0.0001$) and NN/VEH-treated mice ($p < 0.001$) (Fig. 5A,B). Of note, at this time point, NN/MPTP treatment significantly reduced the number of IBA1-positive cells compared with EN/MPTP ($p < 0.001$) (Fig. 5A, B). The results obtained are summarized in Table 1.

3.5. Immunoreactivity of IBA1 in the substantia nigra pars compacta (SNc) following subacute MPTP and Nasco nutriosomes treatment

Subacute MPTP treatment significantly increased the number of IBA1-positive cells in the SNc of the mice sacrificed after either 1 day (number: ~70 %) or 3 days (number: ~39 %) following the last MPTP administration (Fig. 6A-C). Administration of NN (100 mg/kg) markedly contrasted the MPTP-induced elevation in IBA1 immunoreactivity, irrespective of the time of sacrifice (Fig. 6A-C).

Two-way ANOVA revealed significant effects of NN treatment (1 day: $F_{1,31} = 8.599$, $p = 0.0063$; 3 days: $F_{1,30} = 6.694$, $p = 0.0148$), MPTP treatment (1 day: $F_{1,31} = 73.52$, $p < 0.0001$; 3 days: $F_{1,30} = 12.63$, $p = 0.0013$), and NN treatment × MPTP treatment interaction (1 day: $F_{1,31} = 7.209$, $p = 0.0115$; 3 days: $F_{1,30} = 5.524$, $p = 0.0255$) on the total number of IBA1-positive cells.

At 1 day after MPTP treatment, Tukey's post hoc test indicated a significant increase in the number of IBA1-positive cells in mice receiving MPTP in combination with either EN or NN compared with both SAL/VEH- ($p < 0.0001$) and NN/VEH-treated mice ($p < 0.001$) (Fig. 6A-C).

At 3 days after MPTP treatment, Tukey's post hoc test indicated a significant increase in the number of IBA1-positive cells in mice receiving EN/MPTP compared with both SAL/VEH- ($p < 0.0001$) and NN/VEH-treated mice ($p < 0.001$) (Fig. 6A-C). Of note, at both time points, NN/MPTP treatment significantly reduced the number of IBA1-positive cells compared with EN/MPTP ($p < 0.01$) (Fig. 6A-C). The results obtained are summarized in Table 1.

3.6. Co-localization analysis of IBA1 and IL-1β in the caudate-putamen (CPu) following subacute MPTP and Nasco nutriosomes treatment

Subacute MPTP treatment significantly increased IL-1β/IBA1 colocalization in the dorsal CPu of mice sacrificed after either 1 day (~30 %) or 3 days (~28 %) following the last MPTP administration (Fig. 7A-C). At both time points, administration of NN (100 mg/kg) markedly attenuated the MPTP-induced elevation in IL-1β/IBA1 colocalization (Fig. 7A, B).

Two-way ANOVA revealed significant effects of NN treatment (1 day: $F_{1,31} = 10.89$, $p = 0.0024$; 3 days: $F_{1,30} = 13.99$, $p = 0.0008$) and MPTP treatment (1 day: $F_{1,31} = 11.13$, $p = 0.0022$; 3 days: $F_{1,30} = 31.01$, $p < 0.0001$) on IL-1β/IBA1 colocalization. Tukey's post hoc test indicated a significant increase in the IL-1β/IBA1 Manders' correlation coefficient in mice receiving EN/MPTP compared with both SAL/VEH- and NN/VEH-treated mice. This effect was evident at both the 1-day ($p < 0.05$) and 3-day ($p < 0.001$) time points (Fig. 7A, B). Of note, irrespective of the sacrifice time, NN/MPTP treatment significantly reduced the Mander's correlation value compared with EN/MPTP ($p < 0.05$) (Fig. 7A, B). The results obtained are summarized in Table 1.

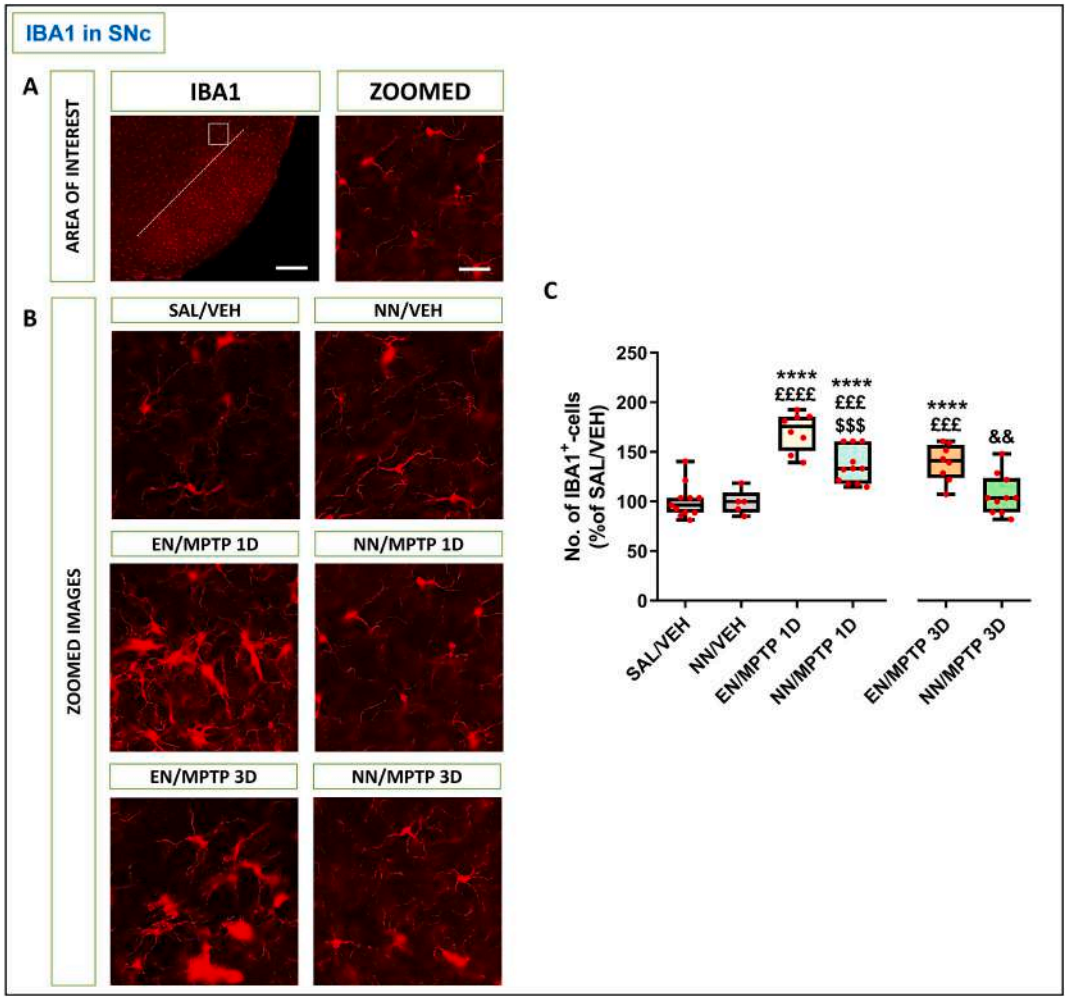

Fig. 6. Effect of NN (100 mg/kg) on the immunoreactivity of ionized calcium-binding adaptor molecule 1 (IBA1) in the substantia nigra pars compacta (SNc) of MPTP-treated mice. (A-B) Representative sections of the SNc immunostained for IBA1. (C) Total number of IBA1-positive cells in the SNc of mice sacrificed either 1 day or 3 days following the last MPTP administration. Values are expressed as a percentage of the SAL/VEH group. Red dots within boxes indicate the values of individual mice. Box plots indicate the top and bottom quartiles; whiskers refer to top and bottom 90 %. ****p < 0.0001 vs. SAL/VEH; $^{£££}p < 0.001$, $^{££££}$p < 0.0001 vs. NN/VEH; $^{\$\$\$}$p < 0.001 vs. EN/MPTP 1D; $^{\&\&}$p < 0.01 vs. EN/MPTP 3D. Scale bar = 500 μm (20×), 10 μm (zoom). D, days; EN: empty nutriosomes; MPTP: 1-methyl-4-phenyl-1,2,3,6-tetrahydropyridine; NN: Nasco nutriosomes; SAL: saline; VEH: vehicle (distilled water). SAL/VEH: *n* = 11; NN/VEH: *n* = 5; EN/MPTP: 1D *n* = 8; NN/MPTP 1D: n = 11; EN/MPTP 3D: n = 8; NN/MPTP 3D: *n* = 10. (For interpretation of the references to colour in this figure legend, the reader is referred to the web version of this article.)

3.7. Colocalization analysis of IBA1 and IL-1β in the substantia nigra pars compacta (SNc) following subacute MPTP and Nasco nutriosomes treatment

Subacute MPTP treatment significantly increased IL-1β/IBA1 colocalization in the SNc of mice sacrificed after either 1 day (~31 %) or 3 days (~23 %) following the last MPTP administration (Fig. 8A-C). Administration of NN (100 mg/kg) exhibited a time-dependent reduction of the MPTP-induced elevation in IL-1β/IBA1 colocalization (Fig. 8A, B).

At 1 day after MPTP treatment, two-way ANOVA revealed significant effects of MPTP treatment ($F_{1,31} = 40.76$, p < 0.0001) on IL-1β/IBA1 colocalization. Tukey's post hoc test indicated a significant increase in the IL-1β/IBA1 Manders' correlation coefficient in mice receiving MPTP in combination with either EN or NN compared with both SAL/VEH- (p < 0.001) and NN/VEH-treated mice (p < 0.01) (Fig. 8A, B).

At 3 days after MPTP treatment, two-way ANOVA revealed significant effects of NN treatment ($F_{1,30} = 5.897$, p = 0.0214), MPTP treatment ($F_{1,30} = 10.89$, p = 0.0025), and NN treatment × MPTP treatment interaction ($F_{1,30} = 6.128$, p = 0.0192) on IL-1β/IBA1 colocalization. Tukey's post hoc test indicated a significant increase in the IL-1β/IBA1 Manders' correlation coefficient in mice receiving EN/MPTP compared with both SAL/VEH- (p < 0.001) and NN/VEH-treated mice (p < 0.01) (Fig. 8A, B). Of note, at this time point, NN/MPTP treatment significantly reduced IL-1β/IBA1 colocalization compared with EN/MPTP (p < 0.01) (Fig. 8A, B). The results obtained are summarized in Table 1.

3.8. Co-localization analysis of IBA1 and TNF-α in the caudate-putamen (CPu) and substantia nigra pars compacta (SNc) following subacute MPTP and Nasco nutriosomes treatment

Subacute MPTP treatment significantly increased TNF-α/IBA1 colocalization in the dorsal CPu of mice sacrificed after either 1 day (~26 %) or 3 days (~24 %) following the last MPTP administration (Fig. 9A-C). At both time points, administration of NN (100 mg/kg) markedly attenuated the MPTP-induced elevation in TNF-α/IBA1 colocalization (Fig. 9A, B). In contrast, MPTP treatment did not induce detectable levels of TNF-α in the SNc, suggesting a region-specific cytokine response to neurotoxic insult **(Supplementary Fig. 1)**.

At 1 day after MPTP treatment, two-way ANOVA revealed significant

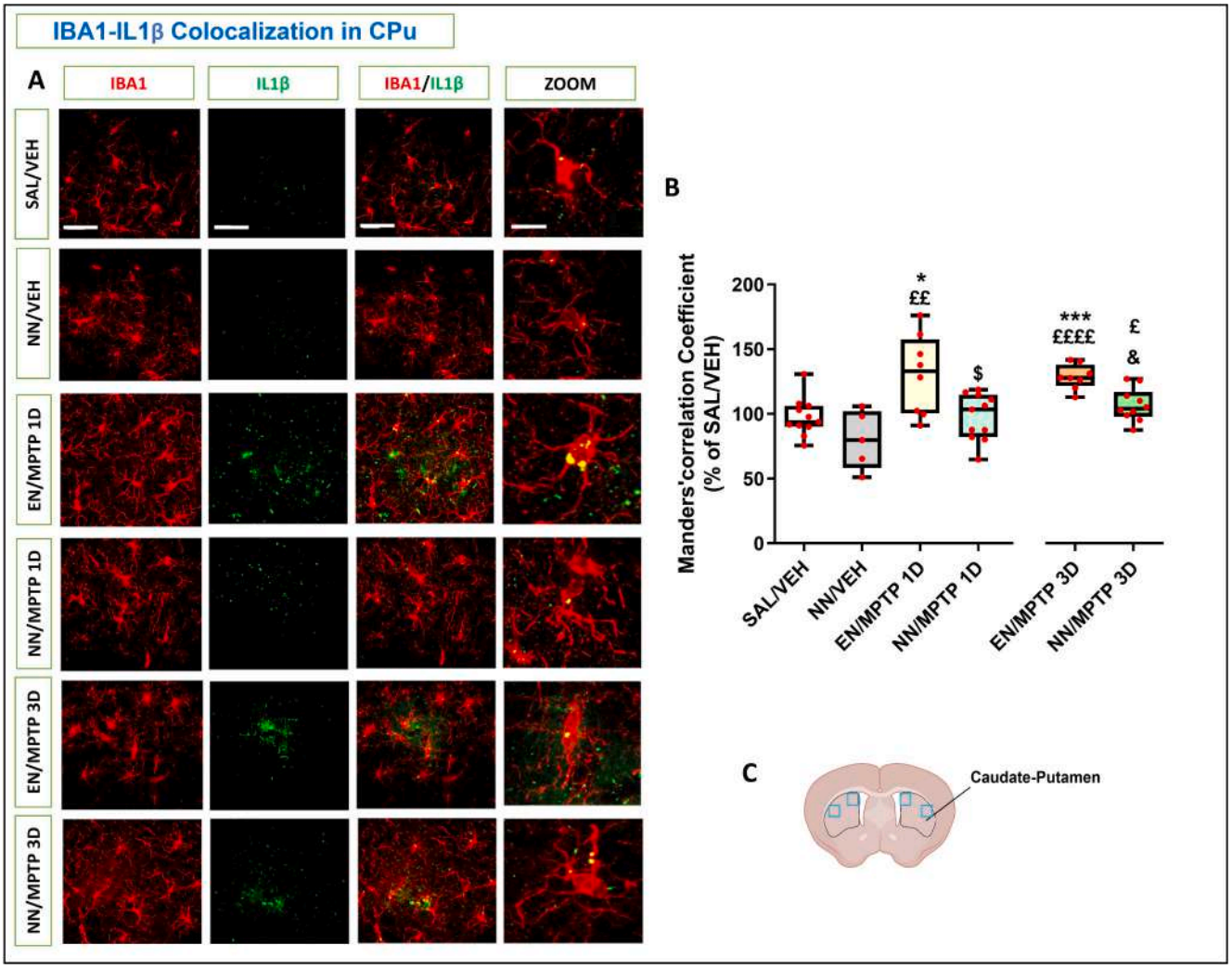

Fig. 7. Effect of NN (100 mg/kg) on interleukin-1β (IL-1β)-ionized calcium-binding adaptor molecule 1 (IBA1) colocalization in the caudate-putamen (CPu) of MPTP-treated mice. (A) Representative confocal images of the dorsomedial CPu immunostained for IL-1β and IBA1. (B) Mander's correlation coefficient in the CPu of mice sacrificed either 1 day or 3 days following the last MPTP administration. (C) Areas of the CPu (blue squares) used for the quantitative analysis. Values are expressed as a percentage of the SAL/VEH group. Red dots within boxes indicate the values of individual mice. Box plots indicate the top and bottom quartiles; whiskers refer to top and bottom 90 %. *$p < 0.05$, ***$p < 0.001$ vs. SAL/VEH; $^{£}p < 0.05$, $^{££}p < 0.01$, $^{££££}p < 0.0001$ vs. NN/VEH; $^{\$}p < 0.05$ vs. EN/MPTP 1D; $^{\&}p < 0.05$ vs. EN/MPTP 3D. Scale bar = 50 μm (63×), 10 μm (zoom). D: day(s) EN: empty nutriosomes; MPTP: 1-methyl-4-phenyl-1,2,3,6-tetrahydropyridine; NN: Nasco nutriosomes; SAL: saline; VEH: vehicle (distilled water). SAL/VEH: $n = 11$; NN/VEH: $n = 5$; EN/MPTP: 1D $n = 8$; NN/MPTP 1D: n = 11; EN/MPTP 3D: n = 8; NN/MPTP 3D: $n = 10$. (For interpretation of the references to colour in this figure legend, the reader is referred to the web version of this article.)

effects of NN treatment ($F_{1,31} = 4.666$, $p = 0.0386$) and MPTP treatment ($F_{1,31} = 6.650$, $p = 0.0149$) on TNF-α/IBA1 colocalization. Tukey's post hoc test indicated a significant increase in the TNF-α/IBA1 Manders' correlation coefficient in mice receiving EN/MPTP compared with both SAL/VEH- ($p < 0.05$) and NN/VEH-treated mice ($p < 0.05$) (Fig. 9A, B). Of note, at this time point, NN/MPTP treatment significantly reduced TNF-α/IBA1 colocalization compared with EN/MPTP ($p < 0.05$) (Fig. 9A, B).

At 3 days after MPTP treatment, two-way ANOVA revealed significant effects of MPTP treatment ($F_{1,30} = 7.151$, $p = 0.0120$) on TNF-α/IBA1 colocalization. Tukey's post hoc test indicated a significant increase in the TNF-α/IBA1 Manders' correlation coefficient in mice receiving EN/MPTP compared with both SAL/VEH- ($p < 0.05$) and NN/VEH-treated mice ($p < 0.05$) (Fig. 9A, B). Although not reaching statistical significance, NN/MPTP treatment exhibited a clear trend toward a reduction in TNF-α/IBA1 colocalization compared to EN/MPTP treatment ($p = 0.174$) (Fig. 9A, B). The results obtained are summarized in Table 1.

4. Discussion

Plant-based extracts have gained attention in the field of neurodegenerative disease research, including PD, due to their multifaceted actions and potential neuroprotective properties. Recently, our group reported that the intragastric delivery of Nasco pomace extract via nutriosomes (NN) significantly protects nigrostriatal dopaminergic neurons against MPTP neurotoxicity in mice (Parekh et al., 2022). This follow-up study provides new insights in this regard, by demonstrating that the intragastric administration of NN (100 mg/kg) in mice significantly contrasts MPTP-induced neuroinflammatory events that may impact on nigrostriatal dopaminergic neurons. Of note, NN's anti-inflammatory effects were found to vary depending on the brain region considered (CPu vs. SNc) and treatment regimen.

Mounting evidence indicates that neuroinflammation plays a significant role in the pathophysiology of PD, contributing to the progressive degeneration of dopaminergic neurons in the SNc (Arena et al., 2022). Increased reactivity of astrocytes and microglial cells and elevated levels of pro-inflammatory cytokines have been consistently

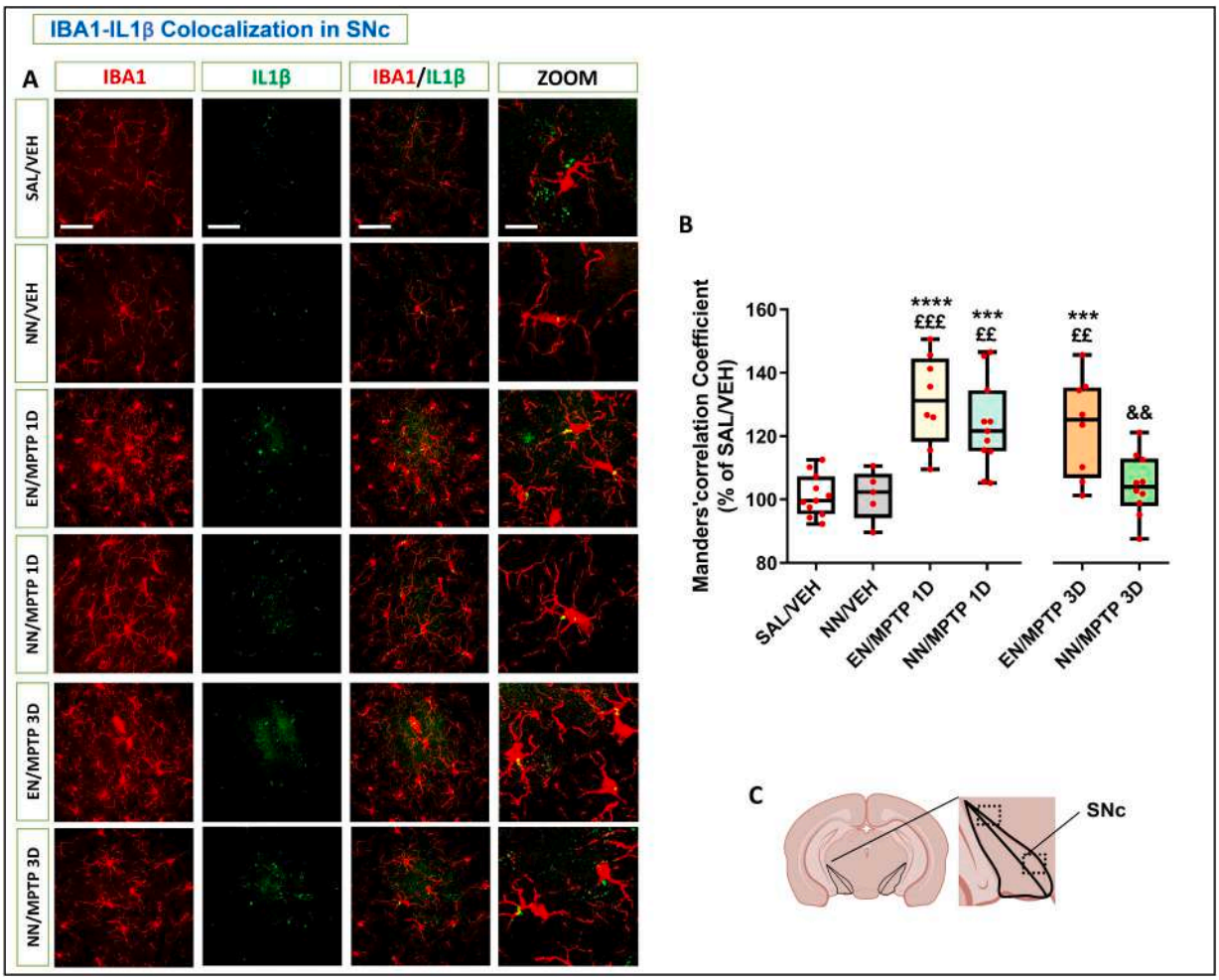

Fig. 8. Effect of NN (100 mg/kg) on interleukin-1β (IL-1β)-ionized calcium-binding adaptor molecule 1 (IBA1) colocalization in the substantia nigra pars compacta (SNc) of MPTP-treated mice. (A) Representative confocal images of the SNc immunostained for IL-1β and IBA1. (B) Mander's correlation coefficient in the SNc of mice sacrificed either 1 day or 3 days following the last MPTP administration. (C) Areas of the SNc (black squares) used for the quantitative analysis. Values are expressed as a percentage of the SAL/VEH group. Red dots within boxes indicate the values of individual mice. Box plots indicate the top and bottom quartiles; whiskers refer to top and bottom 90 %. ***$p < 0.001$, ****$p < 0.0001$ vs. SAL/VEH; $^{\pounds\pounds}p < 0.01$, $^{\pounds\pounds\pounds}p < 0.001$ vs. NN/VEH; $^{\&\&}p < 0.01$ vs. EN/MPTP 3D. Scale bar = 50 μm (63×), 10 μm (zoom). D: day(s); EN: empty nutriosomes; MPTP: 1-methyl-4-phenyl-1,2,3,6-tetrahydropyridine; NN: Nasco nutriosomes; SAL: saline; VEH: vehicle (distilled water). SAL/VEH: $n = 11$; NN/VEH: $n = 5$; EN/MPTP: 1D $n = 8$; NN/MPTP 1D: n = 11; EN/MPTP 3D: n = 8; NN/MPTP 3D: $n = 10$. (For interpretation of the references to colour in this figure legend, the reader is referred to the web version of this article.)

documented in both patients with PD and experimental models of PD (Akiyama and McGeer, 1989; Depino et al., 2003; Rodrigues et al., 2001), including the subacute MPTP mouse model (Costa et al., 2013; Frau et al., 2011) which was chosen for its capacity to induce moderate yet significant neuroinflammation and dopaminergic neurodegeneration, notwithstanding the absence of overt motor deficits (Pupyshev et al., 2019; Santoro et al., 2023). These pathological features closely resemble the presymptomatic stages of PD, rendering them suitable for evaluating the efficacy of pharmacological interventions at preclinical level. Acknowledging the dynamic and transient responses of glial cells to MPTP (Huang et al., 2017), in the present study we evaluated the anti-inflammatory effects of NN at two critical time points, namely, 1 day and 3 days following the last MPTP administration. This approach allowed us to better capture the complex progression of glial activation and identify the time window within which the anti-inflammatory effects of NN may occur.

Regarding astrocytes, we found marked astrogliosis in both the CPu and SNc of mice subjected to subacute MPTP treatment, in line with previous reports from our and other groups (Costa et al., 2013; Frau et al., 2011; Himeda et al., 2006; Zhou et al., 2021). In the CPu, the MPTP-induced astrogliosis was elevated and remained constant at both examined time points, whereas, in the SNc, it displayed a time-dependent pattern, with the highest activation detectable 3 days following the last MPTP administration. Interestingly, repeated combined treatment of NN (100 mg/kg) with MPTP markedly attenuated astrogliosis in the CPu at both 1 day and 3 days following the last MPTP administration. Conversely, in the SNc, NN administration elicited significant effects on reactive astrocytes exclusively in mice sacrificed after 3 days. The varying effectiveness of NN in mitigating MPTP-induced astrogliosis in the CPu and SNc of treated mice is particularly intriguing as it may denote differential responses and vulnerability to neuroinflammatory events across these two brain regions, as previously suggested (Cardoso et al., 2012; Hung and Lee, 1998; Walker et al., 2016). In this regard, it is important to acknowledge the heterogeneous nature of astrocytes, which can exhibit significant phenotypic variations depending on the brain region and microenvironment under consideration (Kostuk et al., 2019; Torres-Ceja and Olsen, 2022). Our findings showing that astrocytes located in the CPu displayed a heightened activation following MPTP compared with those located in the SNc, may underline a phenomenon that likely impacts the antioxidative effects elicited by NN. Consistent with this assumption, NN treatment significantly mitigated astrogliosis in the SNc only 3 days after MPTP

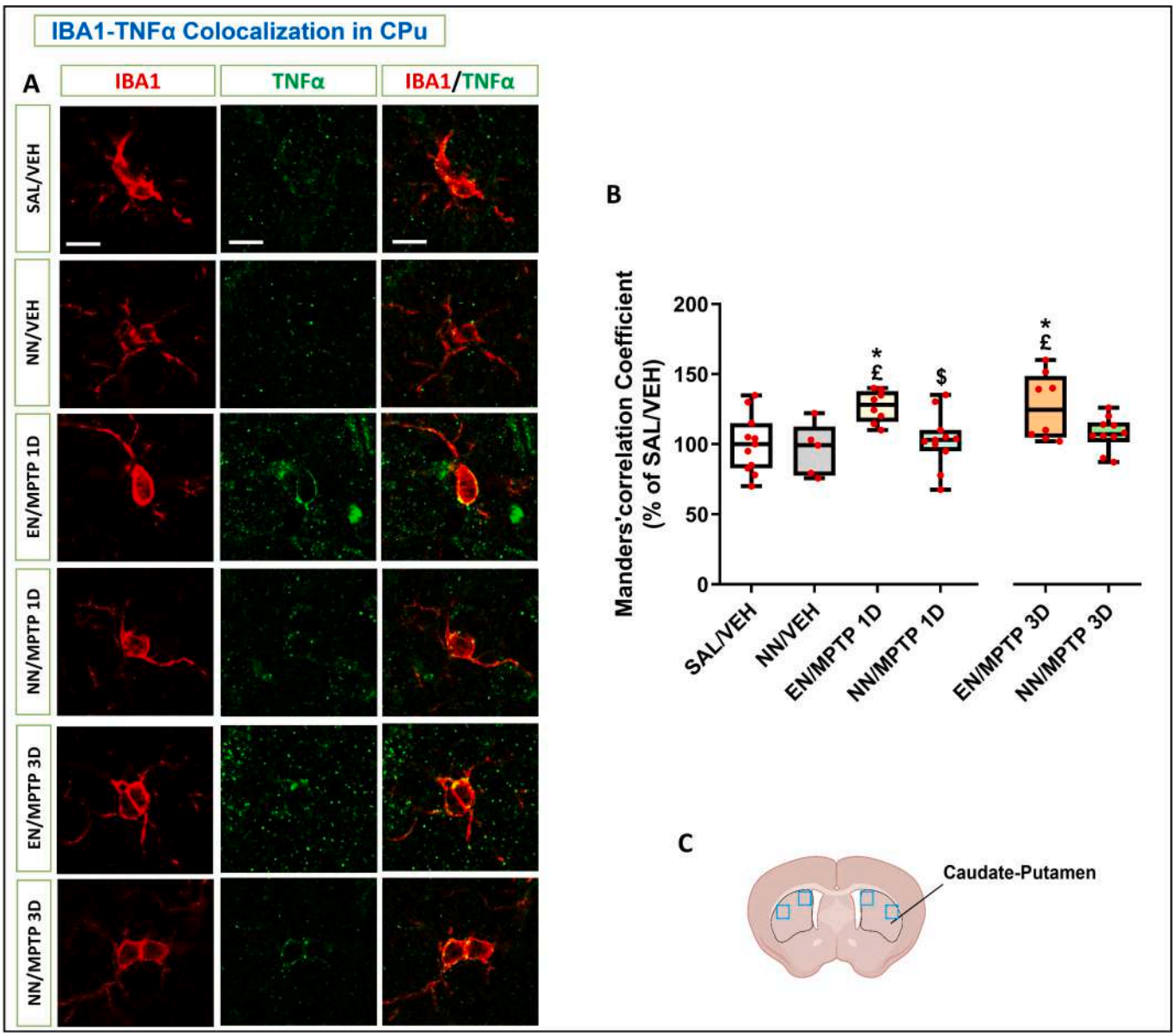

Fig. 9. Effect of NN (100 mg/kg) on tumor necrosis factor alpha (TNF-α)-ionized calcium-binding adaptor molecule 1 (IBA1) colocalization in the caudate-putamen (CPu) of MPTP-treated mice. (A) Representative confocal images of the CPu immunostained for TNF-α and IBA1. (B) Mander's correlation coefficient in the CPu of mice sacrificed either 1 day or 3 days following the last MPTP administration. (C) Areas of the CPu (blue squares) used for the quantitative analysis. Values are expressed as a percentage of the SAL/VEH group. Red dots within boxes indicate the values of individual mice. Box plots indicate the top and bottom quartiles; whiskers refer to top and bottom 90 %. *p < 0.05 vs. SAL/VEH; $^{£}$p < 0.05 vs. NN/VEH; $^{\$}$p < 0.05 vs. EN/MPTP 1D. Scale bar = 10 μm. D: day(s); EN: empty nutriosomes; MPTP: 1-methyl-4-phenyl-1,2,3,6-tetrahydropyridine; NN: Nasco nutriosomes; SAL: saline; VEH: vehicle (distilled water). SAL/VEH: $n = 11$; NN/VEH: $n = 5$; EN/MPTP: 1D $n = 8$; NN/MPTP 1D: n = 11; EN/MPTP 3D: n = 8; NN/MPTP 3D: $n = 10$. (For interpretation of the references to colour in this figure legend, the reader is referred to the web version of this article.)

Table 1
Summary of the effects of NN (100 mg/kg) on the immunoreactivity of glial fibrillary acidic protein (GFAP), ionized calcium-binding adaptor molecule 1 (IBA1), IBA1-interleukin 1β (IL-1β) in the caudate-putamen (CPu) and substantia nigra pars compacta (SNc), and IBA1-Tumor necrosis factor-α (TNF-α) in the CPu of MPTP-treated mice. Legend: N.D., Not Detected.

	Day	GFAP		IBA1		IL-1β/IBA1		TNF-α/IBA1	
		EN/ MPTP	NN/ MPTP	EN/ MPTP	NN/ MPTP	EN/ MPTP	NN/ MPTP	EN/ MPTP	NN/ MPTP
CPu	1	↑	↓	↑↑	↑	↑	↓	↑	↓
	3	↑	↓↓	↑	↓↓	↑	↓	↑	=
SNc	1	↑	↑	↑↑	↓	↑↑	↑	N.D.	N.D.
	3	↑↑	↓↓	↑	↓↓	↑	↓↓	N.D.	N.D.

treatment, when astrogliosis reached its peak.

In addition to assessing the total number of astrocytes in response to treatments, in the present study, we also extended our analysis to morphological aspects of astroglia. Indeed, while in homeostatic conditions, astrocytes assume intricate morphological configurations to establish contact and interact with other cells and cellular components (Baldwin et al., 2023); in pathological conditions, they display a reactive phenotype characterized by cellular rearrangement and the manifestation of distinctive morphological alterations. Therefore, we have evaluated whether NN treatment could also impact the morphological alterations affecting astrocytes following MPTP. In this scope, we conducted a morphological analysis aimed at measuring the number of processes, the total length, and the number of intersections of 3D reconstructed GFAP-positive cells in the CPu and SNc of treated mice. In both brain areas, we found that 3D reconstructed astrocytes exhibited a significantly increased number of processes, total length, and number of intersections when compared with astrocytes of control mice. These morphological changes were evident starting from 1 day after MPTP treatment and persisted after 3 days. Of note, irrespective of the time points considered, we found that NN treatment was unable to modify or rescue any of the morphological parameters observed either in control conditions or following the administration of MPTP, respectively. Therefore, from the present data, we may conclude that NN treatment exerts an impact on astrocytic numerosity rather than morphology and possibly on functional alterations. Nevertheless, it is important to acknowledge that GFAP staining offers information restricted to the cytoskeletal structure of astrocytes, with approximately 85 % of the overall astrocytic surface remaining largely unlabeled (Bushong et al., 2002).

Concerning the other most important component of neuroinflammation, the microglial cells, MPTP treatment led to a significant increase in the total number of IBA1-positive cells in both the CPu and SNc of treated mice, at the two examined time points. These findings are consistent with immunohistochemical data obtained from the CPu and SNc of mice subjected to similar regimens of subacute MPTP treatment and interval of sacrifice from the last MPTP administration (Kim et al., 2013; Ramos-Molina et al., 2023; Yu et al., 2015). Specifically, we found about 31 % and 71 % increase in the number of IBA1-positive cells in the CPu and SNc, respectively, 1 day after MPTP administration. This increase was found to be about 23 % (CPu) and 39 % (SNc) at the 3-day time point. These findings are in line with prior data indicating rapid and transient microgliosis following brain injury (Liberatore et al., 1999; Wang et al., 2012). Importantly, in the SNc, NN treatment markedly counteracted the increase in the number of IBA1-positive cells induced by MPTP, regardless of the specific time points considered. In contrast, in the CPu, the anti-inflammatory effects induced by NN were significant in mice sacrificed 3 days after the last administration of MPTP, while a trend toward reduction was observed 1 day after MPTP treatment. Taking into account previous evidence supporting the causative role of microgliosis in dopaminergic neuron degeneration (Joers et al., 2017; Stefanova, 2022) and the neuroprotective effects of NN treatment previously observed by our group in mice subjected to subacute MPTP treatment (Parekh et al., 2022), the current findings suggest that the neuroprotective actions of NN may, to some extent, be ascribed to the anti-inflammatory effects exerted by the NN treatment on reactive microglial cells in the SNc and CPu. In support of this assumption, previous studies conducted in in vitro and in vivo models of neurodegenerative and neuroinflammatory diseases, including PD, have demonstrated that the administration of individual polyphenols, known to be present in Nasco pomace extract (e.g., gallic acid, catechin, epicatechin, or quercetin) (Parekh et al., 2022), yields neuroprotective effects by counteracting neuroinflammation (Bournival et al., 2012; Chen et al., 2022; Huang et al., 2005; Kita et al., 2014; Liu et al., 2020) and reducing microglial reactivity (Fan et al., 2019; Huang et al., 2024; Qu et al., 2022).

Lastly, in the present study, we explored the impact of NN treatment on the microglial production of the pro-inflammatory cytokines TNF-α and IL-1β. This choice was grounded in the cytokine's ability to initiate and amplify neuroinflammatory responses, thereby contributing to the severity of various neurodegenerative disorders (Leal et al., 2013; Mendiola and Cardona, 2018). Although astrocytes and neurons can also produce TNF-α and IL-1β under inflammatory conditions (Acarin et al., 2000; Chung and Benveniste, 1990; Gahring et al., 1996), microglia are recognized as the primary responders and major sources of these cytokines in the CNS (Leal et al., 2013). In the context of PD, elevated levels of TNF-α and IL-1β have been reported in the CSF (Majbour et al., 2020; Mogi et al., 1996), CPu (Mogi et al., 1994), SN (Hunot et al., 1999), and serum (Xiromerisiou et al., 2022) of patients with PD.

Regarding TNF-α, elevated levels of this cytokine have been correlated with non-motor symptoms in PD patients (Menza et al., 2010). Moreover, genetically manipulated mice lacking either TNF-α or TNF receptors show protection against MPTP-induced dopaminergic neurotoxicity, highlighting the critical role of TNF-α in dopaminergic neurodegeneration (Ferger et al., 2004; Rousselet et al., 2002; Sriram et al., 2002). Consequently, inhibition of TNF-α signaling, particularly in the early stages of PD, is regarded as a promising therapeutic approach for modifying the disease course (Amin et al., 2022).

In the CPu, we found a significant elevation in TNF-α/IBA1 colocalization in MPTP-treated mice compared with controls. This elevation was evident at both 1 and 3 days from the last MPTP administration. These results align with previous studies indicating an overall elevation in striatal TNF-α protein levels in mice exposed to different MPTP treatment regimens (Borrajo et al., 2014; Luchtman et al., 2009, 2012). Importantly, in this brain region, while NN treatment significantly reduced TNF-α/IBA1 colocalization at 1 day, a trend toward reduction was observed at 3 days following the last MPTP administration. Although further research is needed to fully elucidate the underlying mechanisms, these findings support the evidence that phytochemicals derived from natural sources may effectively mitigate neuroinflammation by inhibiting the TNF-α signaling (Subedi et al., 2020; Zahedipour et al., 2022).

In contrast to the CPu, TNF-α immunoreactivity was undetectable in the SNc of mice, regardless of the treatment administered or the time of sacrifice. While this result may seem unexpected, it is consistent with previous studies showing that TNF-α expression in the ventral midbrain declines rapidly following acute MPTP treatment (Rabaneda-Lombarte et al., 2021). Moreover, TNF-α mRNA levels were below the detection limit in the unilateral 6-OHDA rat model of PD (Depino et al., 2003). In contrast, in the moderate-to-severe subchronic MPTP plus probenecid mouse model of PD, the demise of dopaminergic neurons in the SNc was found to parallel the increase in TNF-α/IBA1 colocalization (Pisanu et al., 2014). These findings suggest that the severity and persistence of neurotoxic insults are crucial factors influencing TNF-α production by microglial cells in the SNc. Besides, It is also noteworthy that aberrant TNF-α levels appear to predominantly affect dopaminergic function in the CPu. For instance, TNF-α knockout mice showed reduced dopamine loss in the CPu following MPTP treatment, without significant changes in the number of TH-positive neurons in the SNc (Ferger et al., 2004). These regional and temporal characteristics of TNF-α further underscore the complexity of neuroinflammatory responses in PD, emphasizing the importance of tailored therapeutic approaches.

Regarding IL-1β, a previous study performed in rats subsequently exposed to a non-toxic dose of lipopolysaccharide in the SNc and 6-hydroxydopamine in the CPu, indicated that the heightened vulnerability found in nigrostriatal dopaminergic neurons was principally mediated by the IL-1β released by microglial cells (Koprich et al., 2008).

Consistent with prior observations in MPTP-treated mice (Khan et al., 2013; Yarim et al., 2022), protein levels of IL-1β were significantly increased within microglial cells from MPTP-treated mice compared with controls. This increase was found in both the CPu and SNc, reaching its peak 1 day after the last MPTP administration. Importantly, we observed that NN treatment attenuates the MPTP-induced microglial

production of IL-1β depending on the brain area considered and the time of sacrifice. Indeed, in the CPu, NN treatment significantly reduced the IL-1β/IBA1 colocalization at both time points. On the other hand, in the SNc, NN treatment contrasted the microglial production of IL-1β exclusively in mice sacrificed 3 days after MPTP treatment. Once more, these results substantiate the perspective that the SNc and the CPu may exhibit a differential susceptibility toward MPTP effects, with the SNc potentially requiring a longer duration of NN treatment to counteract MPTP-induced neuroinflammatory processes. In this regard, it is noteworthy that several neuropathological studies conducted on patients and preclinical models of PD converge in suggesting differential vulnerabilities to neurotoxic insults between dopaminergic cell bodies in the SNc and synaptic terminals in the CPu. Specifically, it has been proposed that PD initiates with the early manifestation of synaptic impairments, succeeded by the loss of dopaminergic axons and terminations within the CPu, and subsequently advances through the involvement of mesencephalic cell bodies (Gcwensa et al., 2021; Imbriani et al., 2018; Schirinzi et al., 2016). Hence, the anti-inflammatory effects induced by NN treatment in the CPu of MPTP-treated mice may play a crucial role in more effectively counteracting the propagation of neurotoxic events impacting the dopaminergic nigrostriatal tract. Regarding the mechanisms potentially involved in NN-mediated reduction of IL-1β levels, previous evidence suggests that several natural polyphenols, such as curcumin, resveratrol, and quercetin, the latter of which is contained in NN (Parekh et al., 2022), may reduce the microglial production of pro-inflammatory cytokines by modulating the nuclear factor kappa B (NF-kB) pathway (Karunaweera et al., 2015). Nevertheless, additional investigations are necessary to substantiate the hypothesis stated and verify the mechanisms involved.

In conclusion, the present research, extended the previous findings of our group on the neuroprotective effects of NN in a subacute MPTP mouse model of PD (Parekh et al., 2022), by providing consistent evidence supporting the anti-inflammatory effects of NN. In this respect, NN treatment significantly mitigates MPTP-induced astrogliosis and microgliosis, as well as the microglial production of the pro-inflammatory cytokines TNF-α and IL-1β. Notably, the anti-inflammatory effects of NN were more pronounced in the CPu compared with the SNc, which may be very relevant in light of compelling evidence indicating dopaminergic terminals as the primary site implicated in the early pathological cascades of the disease (Gcwensa et al., 2021; Imbriani et al., 2018; Schirinzi et al., 2016). The results also demonstrate that nutriosome formulation, an innovative nano-drug delivery system for in vivo administration, increases the bioavailability of otherwise inactive molecules (Parekh et al., 2022). Moreover, as neuroinflammation is implicated in the demise of nigrostriatal dopaminergic neurons, these findings may provide a potential mechanism underlying the neuroprotective effects observed upon NN treatment in the subacute MPTP mouse model of PD. Future studies will be fundamental in elucidating the contribution of each major polyphenol present in the Nasco pomace extract to its anti-inflammatory and neuroprotective effects, as well as in providing a more comprehensive understanding of the underlying molecular mechanisms involved.

Funding source

The present study was supported by grants from the Italian Ministry of University and Research (PRIN#2015R9ASHT, PI: MiM; PRIN #2017LYTE9M, PI: MiM), the CNR project “Nutrage” - FOE 2021, DBA. AD005.225 (IN-CA, Co-PI: AP), and by the POC project “Nutriosomi e scarti agro-industriali per il controllo di disbiosi intestinali, stress ossidativo, e declino cognitivo. NUTRINNOVA” of the University of Cagliari (PI: MaM, AP). MS gratefully thanks the Zardi-Gori Foundation for the financial support (research grant 2021).

CRediT authorship contribution statement

Pathik Parekh: Methodology, Investigation, Formal analysis, Data curation, Writing – original draft. **Marcello Serra:** Supervision, Methodology, Investigation, Formal analysis, Data curation, Conceptualization, Writing – original draft. **Mohamad Allaw:** Methodology, Investigation. **Matteo Perra:** Methodology, Investigation. **Annalisa Pinna:** Supervision, Project administration, Funding acquisition, Writing – review & editing. **Maria Manconi:** Supervision, Project administration, Funding acquisition, Writing – review & editing. **Micaela Morelli:** Supervision, Project administration, Funding acquisition, Conceptualization, Writing – review & editing, Writing – original draft.

Declaration of competing interest

The authors declare that they have no known competing financial interests or personal relationships that could have appeared to influence the work reported in this paper.

Data availability

Data will be made available on request.

Acknowledgements

PP, MS, MM, AP thank the Centre for Research University Services (CeSAR) and the “Centro Servizi di Ateneo per gli Stabulari” (CeSASt), for the technical support. The authors acknowledge Medica-Edit for their assistance in revising the English language of this manuscript. PP is supported in part by NIA, NIH, Baltimore, MD, USA.

Appendix A. Supplementary data

Supplementary data to this article can be found online at https://doi.org/10.1016/j.expneurol.2024.114958.

References

Acarin, L., González, B., Castellano, B., 2000. Neuronal, astroglial and microglial cytokine expression after an excitotoxic lesion in the immature rat brain. Eur. J. Neurosci. 12, 3505–3520. https://doi.org/10.1046/j.1460-9568.2000.00226.x.

Akiyama, H., McGeer, P.L., 1989. Microglial response to 6-hydroxydopamine-induced substantia nigra lesions. Brain Res. 489, 247–253. https://doi.org/10.1016/0006-8993(89)90857-3.

Allaw, M., Manca, M.L., Caddeo, C., Recio, M.C., Pérez-Brocal, V., Moya, A., Fernàndez-Busquets, X., Manconi, M., 2020. Advanced strategy to exploit wine-making waste by manufacturing antioxidant and prebiotic fibre-enriched vesicles for intestinal health. Colloids Surf. B: Biointerfaces 193, 111146. https://doi.org/10.1016/j.colsurfb.2020.111146.

Amin, R., Quispe, C., Docea, A.O., Ydyrys, A., Kulbayeva, M., Durna Daştan, S., Calina, D., Sharifi-Rad, J., 2022. The role of tumour necrosis factor in neuroinflammation associated with Parkinson’s disease and targeted therapies. Neurochem. Int. 158, 105376. https://doi.org/10.1016/j.neuint.2022.105376.

Andoh, M., Koyama, R., 2021. Microglia regulate synaptic development and plasticity. Dev. Neurobiol. 81, 568–590. https://doi.org/10.1002/dneu.22814.

Arena, G., Sharma, K., Agyeah, G., Krüger, R., Grünewald, A., Fitzgerald, J.C., 2022. Neurodegeneration and Neuroinflammation in Parkinson’s disease: a self-sustained loop. Curr. Neurol. Neurosci. Rep. 22, 427–440. https://doi.org/10.1007/s11910-022-01207-5.

Baldwin, K.T., Murai, K.K., Khakh, B.S., 2023. Astrocyte morphology. Trends Cell Biol. https://doi.org/10.1016/j.tcb.2023.09.006. S0962892423002040.

Bolte, S., Cordelières, F.P., 2006. A guided tour into subcellular colocalization analysis in light microscopy. J. Microsc. 224, 213–232. https://doi.org/10.1111/j.1365-2818.2006.01706.x.

Bondi, H., Bortolotto, V., Canonico, P.L., Grilli, M., 2021. Complex and regional-specific changes in the morphological complexity of GFAP+ astrocytes in middle-aged mice. Neurobiol. Aging 100, 59–71. https://doi.org/10.1016/j.neurobiolaging.2020.12.018.

Borrajo, A., Rodriguez-Perez, A.I., Diaz-Ruiz, C., Guerra, M.J., Labandeira-Garcia, J.L., 2014. Microglial TNF-α mediates enhancement of dopaminergic degeneration by brain angiotensin. Glia 62, 145–157. https://doi.org/10.1002/glia.22595.

Bournival, J., Plouffe, M., Renaud, J., Provencher, C., Martinoli, M.-G., 2012. Quercetin and Sesamin protect dopaminergic cells from MPP $^{+}$ -induced Neuroinflammation in

a microglial (N9)-neuronal (PC12) Coculture system. Oxidative Med. Cell. Longev. 2012, 1–11. https://doi.org/10.1155/2012/921941.
Bushong, E.A., Martone, M.E., Jones, Y.Z., Ellisman, M.H., 2002. Protoplasmic astrocytes in CA1 stratum Radiatum occupy separate anatomical domains. J. Neurosci. 22, 183–192. https://doi.org/10.1523/JNEUROSCI.22-01-00183.2002.
Cardoso, H.D., Passos, P.P., Lagranha, C.J., Ferraz, A.C., Santos Júnior, E.F., Oliveira, R. S., Oliveira, P.E.L., Santos, R.D.C.F., Santana, D.F., Borba, J.M.C., Rocha-de-Melo, A. P., Guedes, R.C.A., Navarro, D.M.A.F., Santos, G.K.N., Borner, R., Picanço-Diniz, C. W., Beltrão, E.I., Silva, J.F., Rodrigues, M.C.A., Andrade Da Costa, B.L.S., 2012. Differential vulnerability of substantia nigra and corpus striatum to oxidative insult induced by reduced dietary levels of essential fatty acids. Front. Hum. Neurosci. 6. https://doi.org/10.3389/fnhum.2012.00249.
Cebrián, C., Loike, J.D., Sulzer, D., 2014. Neuroinflammation in Parkinson's disease animal models: A cell stress response or a step in neurodegeneration? In: Nguyen, H. H.P., Cenci, M.A. (Eds.), Behavioral Neurobiology of Huntington's Disease and Parkinson's Disease, Current Topics in Behavioral Neurosciences. Springer, Berlin Heidelberg, Berlin, Heidelberg, pp. 237–270. https://doi.org/10.1007/7854_2014_356.
Chen, G., Cheng, K., Niu, Y., Zhu, L., Wang, X., 2022. (−)-Epicatechin gallate prevents inflammatory response in hypoxia-activated microglia and cerebral edema by inhibiting NF-κB signaling. Arch. Biochem. Biophys. 729, 109393. https://doi.org/10.1016/j.abb.2022.109393.
Cheng, H., Ulane, C.M., Burke, R.E., 2010. Clinical progression in Parkinson disease and the neurobiology of axons. Ann. Neurol. 67, 715–725. https://doi.org/10.1002/ana.21995.
Chung, I.Y., Benveniste, E.N., 1990. Tumor necrosis factor-alpha production by astrocytes. Induction by lipopolysaccharide, IFN-gamma, and IL-1 beta. J. Immunol. 144, 2999–3007.
Costa, G., Frau, L., Wardas, J., Pinna, A., Plumitallo, A., Morelli, M., 2013. MPTP-induced dopamine neuron degeneration and glia activation is potentiated in MDMA-pretreated mice. Mov. Disord. 28, 1957–1965. https://doi.org/10.1002/mds.25646.
Depino, A.M., Earl, C., Kaczmarczyk, E., Ferrari, C., Besedovsky, H., Del Rey, A., Pitossi, F.J., Oertel, W.H., 2003. Microglial activation with atypical proinflammatory cytokine expression in a rat model of Parkinson's disease. Eur. J. Neurosci. 18, 2731–2742. https://doi.org/10.1111/j.1460-9568.2003.03014.x.
Dunn, K.W., Kamocka, M.M., McDonald, J.H., 2011. A practical guide to evaluating colocalization in biological microscopy. Am. J. Phys. Cell Phys. 300, C723–C742. https://doi.org/10.1152/ajpcell.00462.2010.
Fan, H., Tang, H.-B., Shan, L.-Q., Liu, S.-C., Huang, D.-G., Chen, X., Chen, Z., Yang, M., Yin, X.-H., Yang, H., Hao, D.-J., 2019. Quercetin prevents necroptosis of oligodendrocytes by inhibiting macrophages/microglia polarization to M1 phenotype after spinal cord injury in rats. J. Neuroinflammation 16, 206. https://doi.org/10.1186/s12974-019-1613-2.
Ferger, B., Leng, A., Mura, A., Hengerer, B., Feldon, J., 2004. Genetic ablation of tumor necrosis factor-alpha (*TNF-α*) and pharmacological inhibition of TNF-synthesis attenuates MPTP toxicity in mouse striatum. J. Neurochem. 89, 822–833. https://doi.org/10.1111/j.1471-4159.2004.02399.x.
Ferreira, T.A., Blackman, A.V., Oyrer, J., Jayabal, S., Chung, A.J., Watt, A.J., Sjöström, P. J., Van Meyel, D.J., 2014. Neuronal morphometry directly from bitmap images. Nat. Methods 11, 982–984. https://doi.org/10.1038/nmeth.3125.
Franklin, K., Paxinos, G., 2008. The Mouse Brain in Stereotaxic Coordinates, Compact - 3rd edition. Academic press, pp. 1–256.
Frau, L., Borsini, F., Wardas, J., Khairnar, A.S., Schintu, N., Morelli, M., 2011. Neuroprotective and anti-inflammatory effects of the adenosine a $_{2A}$ receptor antagonist ST1535 in a MPTP mouse model of Parkinson's disease. Synapse 65, 181–188. https://doi.org/10.1002/syn.20833.
Gahring, L.C., Carlson, N.G., Kulmer, R.A., Rogers, S.W., 1996. Neuronal expression of tumor necrosis factor alpha in the OVOUJI fme brain. Neuroimmunomodulation 3, 289–303. https://doi.org/10.1159/000097283.
Gcwensa, N.Z., Russell, D.L., Cowell, R.M., Volpicelli-Daley, L.A., 2021. Molecular mechanisms underlying synaptic and axon degeneration in Parkinson's disease. Front. Cell. Neurosci. 15, 626128. https://doi.org/10.3389/fncel.2021.626128.
Gelders, G., Baekelandt, V., Van Der Perren, A., 2018. Linking Neuroinflammation and neurodegeneration in Parkinson's disease. J Immunol Res 2018, 1–12. https://doi.org/10.1155/2018/4784268.
Himeda, T., Watanabe, Y., Tounai, H., Hayakawa, N., Kato, H., Araki, T., 2006. Time dependent alterations of co-localization of S100β and GFAP in the MPTP-treated mice. J. Neural Transm. 113, 1887–1894. https://doi.org/10.1007/s00702-006-0482-x.
Huang, Q., Wu, L.-J., Tashiro, S., Gao, H.-Y., Onodera, S., Ikejima, T., 2005. (+)-Catechin, an ingredient of green tea, protects murine microglia from oxidative stress-induced DNA damage and cell cycle arrest. J. Pharmacol. Sci. 98, 16–24. https://doi.org/10.1254/jphs.FPJ04053X.
Huang, D., Xu, J., Wang, J., Tong, J., Bai, X., Li, H., Wang, Z., Huang, Y., Wu, Y., Yu, M., Huang, F., 2017. Dynamic changes in the nigrostriatal pathway in the MPTP mouse model of Parkinson's disease. In: Parkinson's Disease, 2017, pp. 1–7. https://doi.org/10.1155/2017/9349487.
Huang, J., Jiang, Z., Wu, M., Zhang, J., Chen, C., 2024. Gallic acid exerts protective effects in spinal cord injured rats through modulating microglial polarization. Physiol. Behav. 273, 114405. https://doi.org/10.1016/j.physbeh.2023.114405.
Hung, H.-C., Lee, E.H.Y., 1998. MPTP produces differential oxidative stress and Antioxidative responses in the nigrostriatal and mesolimbic dopaminergic pathways. Free Radic. Biol. Med. 24, 76–84. https://doi.org/10.1016/S0891-5849(97)00206-2.
Hunot, S., Dugas, N., Faucheux, B., Hartmann, A., Tardieu, M., Debré, P., Agid, Y., Dugas, B., Hirsch, E.C., 1999. FcεRII/CD23 is expressed in Parkinson's disease and induces, *in vitro,* production of nitric oxide and tumor necrosis factor-α in glial cells. J. Neurosci. 19, 3440–3447. https://doi.org/10.1523/JNEUROSCI.19-09-03440.1999.
Imbriani, P., Schirinzi, T., Meringolo, M., Mercuri, N.B., Pisani, A., 2018. Centrality of early Synaptopathy in Parkinson's disease. Front. Neurol. 9, 103. https://doi.org/10.3389/fneur.2018.00103.
Joers, V., Tansey, M.G., Mulas, G., Carta, A.R., 2017. Microglial phenotypes in Parkinson's disease and animal models of the disease. Prog. Neurobiol. 155, 57–75. https://doi.org/10.1016/j.pneurobio.2016.04.006.
Jurcau, A., Andronie-Cioara, F.L., Nistor-Cseppento, D.C., Pascalau, N., Rus, M., Vasca, E., Jurcau, M.C., 2023. The involvement of Neuroinflammation in the onset and progression of Parkinson's disease. IJMS 24, 14582. https://doi.org/10.3390/ijms241914582.
Karunaweera, N., Raju, R., Gyengesi, E., Münch, G., 2015. Plant polyphenols as inhibitors of NF-κB induced cytokine production—a potential anti-inflammatory treatment for Alzheimer's disease? Front. Mol. Neurosci. 8. https://doi.org/10.3389/fnmol.2015.00024.
Khan, M.M., Kempuraj, D., Thangavel, R., Zaheer, A., 2013. Protection of MPTP-induced neuroinflammation and neurodegeneration by Pycnogenol. Neurochem. Int. 62, 379–388. https://doi.org/10.1016/j.neuint.2013.01.029.
Kim, B.K., Shin, E.-J., Kim, H.-C., Chung, Y.H., Dang, D.-K., Jung, B.-D., Park, D.-H., Wie, M.B., Kim, W.-K., Shimizu, T., Nabeshima, T., Jeong, J.H., 2013. Platelet-activating factor receptor knockout mice are protected from MPTP-induced dopaminergic degeneration. Neurochem. Int. 63, 121–132. https://doi.org/10.1016/j.neuint.2013.05.010.
Kita, T., Asanuma, M., Miyazaki, I., Takeshima, M., 2014. Protective effects of phytochemical antioxidants against neurotoxin-induced degeneration of dopaminergic neurons. J. Pharmacol. Sci. 124, 313–319. https://doi.org/10.1254/jphs.13R19CP.
Koprich, J.B., Reske-Nielsen, C., Mithal, P., Isacson, O., 2008. Neuroinflammation mediated by IL-1β increases susceptibility of dopamine neurons to degeneration in an animal model of Parkinson's disease. J. Neuroinflammation 5, 8. https://doi.org/10.1186/1742-2094-5-8.
Kostuk, E.W., Cai, J., Iacovitti, L., 2019. Subregional differences in astrocytes underlie selective neurodegeneration or protection in Parkinson's disease models in culture. Glia 67, 1542–1557. https://doi.org/10.1002/glia.23627.
Leal, M.C., Casabona, J.C., Puntel, M., Pitossi, F.J., 2013. Interleukin-1β and tumor necrosis factor-α: reliable targets for protective therapies in Parkinson's disease? Front. Cell. Neurosci. 7. https://doi.org/10.3389/fncel.2013.00053.
Liberatore, G.T., Jackson-Lewis, V., Vukosavic, S., Mandir, A.S., Vila, M., McAuliffe, W. G., Dawson, V.L., Dawson, T.M., Przedborski, S., 1999. Inducible nitric oxide synthase stimulates dopaminergic neurodegeneration in the MPTP model of Parkinson disease. Nat. Med. 5, 1403–1409. https://doi.org/10.1038/70978.
Liu, Y.-L., Hsu, C.-C., Huang, H.-J., Chang, C.-J., Sun, S.-H., Lin, A.M.-Y., 2020. Gallic acid attenuated LPS-induced Neuroinflammation: protein aggregation and necroptosis. Mol. Neurobiol. 57, 96–104. https://doi.org/10.1007/s12035-019-01759-7.
Liu, T.-W., Chen, C.-M., Chang, K.-H., 2022. Biomarker of Neuroinflammation in Parkinson's disease. IJMS 23, 4148. https://doi.org/10.3390/ijms23084148.
Lombardo, D., Kiselev, M.A., 2022. Methods of liposomes preparation: formation and control factors of versatile Nanocarriers for biomedical and nanomedicine application. Pharmaceutics 14, 543. https://doi.org/10.3390/pharmaceutics14030543.
Luchtman, D.W., Shao, D., Song, C., 2009. Behavior, neurotransmitters and inflammation in three regimens of the MPTP mouse model of Parkinson's disease. Physiol. Behav. 98, 130–138. https://doi.org/10.1016/j.physbeh.2009.04.021.
Luchtman, D.W., Meng, Q., Song, C., 2012. Ethyl-eicosapentaenoate (E-EPA) attenuates motor impairments and inflammation in the MPTP-probenecid mouse model of Parkinson's disease. Behav. Brain Res. 226, 386–396. https://doi.org/10.1016/j.bbr.2011.09.033.
Majbour, N.K., Aasly, J.O., Hustad, E., Thomas, M.A., Vaikath, N.N., Elkum, N., Van De Berg, W.D.J., Tokuda, T., Mollenhauer, B., Berendse, H.W., El-Agnaf, O.M.A., 2020. CSF total and oligomeric α-Synuclein along with TNF-α as risk biomarkers for Parkinson's disease: a study in LRRK2 mutation carriers. Transl. Neurodegener. 9, 15. https://doi.org/10.1186/s40035-020-00192-4.
Manconi, M., Caddeo, C., Manca, M.L., Fadda, A.M., 2020. Oral delivery of natural compounds by phospholipid vesicles. Nanomedicine (London) 15, 1795–1803. https://doi.org/10.2217/nnm-2020-0085.
McGeer, P.L., Itagaki, S., Boyes, B.E., McGeer, E.G., 1988. Reactive microglia are positive for HLA-DR in the substantia nigra of Parkinson's and Alzheimer's disease brains. Neurology 38. https://doi.org/10.1212/WNL.38.8.1285, 1285–1285.
Mendiola, A.S., Cardona, A.E., 2018. The IL-1β phenomena in neuroinflammatory diseases. J. Neural Transm. 125, 781–795. https://doi.org/10.1007/s00702-017-1732-9.
Menza, M., Dobkin, R.D., Marin, H., Mark, M.H., Gara, M., Bienfait, K., Dicke, A., Kusnekov, A., 2010. The role of inflammatory cytokines in cognition and other non-motor symptoms of Parkinson's disease. Psychosomatics 51, 474–479. https://doi.org/10.1176/appi.psy.51.6.474.
Mogi, M., Harada, M., Kondo, T., Riederer, P., Inagaki, H., Minami, M., Nagatsu, T., 1994. Interleukin-1β, interleukin-6, epidermal growth factor and transforming growth factor-α are elevated in the brain from parkinsonian patients. Neurosci. Lett. 180, 147–150. https://doi.org/10.1016/0304-3940(94)90508-8.
Mogi, M., Harada, M., Narabayashi, H., Inagaki, H., Minami, M., Nagatsu, T., 1996. Interleukin (IL)-1β, IL-2, IL-4, IL-6 and transforming growth factor-α levels are elevated in ventricular cerebrospinal fluid in juvenile parkinsonism and Parkinson's

disease. Neurosci. Lett. 211, 13–16. https://doi.org/10.1016/0304-3940(96)12706-3.
Obeso, J.A., Stamelou, M., Goetz, C.G., Poewe, W., Lang, A.E., Weintraub, D., Burn, D., Halliday, G.M., Bezard, E., Przedborski, S., Lehericy, S., Brooks, D.J., Rothwell, J.C., Hallett, M., DeLong, M.R., Marras, C., Tanner, C.M., Ross, G.W., Langston, J.W., Klein, C., Bonifati, V., Jankovic, J., Lozano, A.M., Deuschl, G., Bergman, H., Tolosa, E., Rodriguez-Violante, M., Fahn, S., Postuma, R.B., Berg, D., Marek, K., Standaert, D.G., Surmeier, D.J., Olanow, C.W., Kordower, J.H., Calabresi, P., Schapira, A.H.V., Stoessl, A.J., 2017. Past, present, and future of Parkinson's disease: a special essay on the 200th anniversary of the shaking palsy. Mov. Disord. 32, 1264–1310. https://doi.org/10.1002/mds.27115.
Ouchi, Y., Yoshikawa, E., Sekine, Y., Futatsubashi, M., Kanno, T., Ogusu, T., Torizuka, T., 2005. Microglial activation and dopamine terminal loss in early Parkinson's disease. Ann. Neurol. 57, 168–175. https://doi.org/10.1002/ana.20338.
Pardo-Moreno, T., García-Morales, V., Suleiman-Martos, S., Rivas-Domínguez, A., Mohamed-Mohamed, H., Ramos-Rodríguez, J.J., Melguizo-Rodríguez, L., González-Acedo, A., 2023. Current treatments and new, tentative therapies for Parkinson's Disease. Pharmaceutics 15, 770. https://doi.org/10.3390/pharmaceutics15030770.
Parekh, P., Serra, M., Allaw, M., Perra, M., Marongiu, J., Tolle, G., Pinna, A., Casu, M.A., Manconi, M., Caboni, P., Manzoni, O.J.J., Morelli, M., 2022. Characterization of Nasco grape pomace-loaded nutriosomes and their neuroprotective effects in the MPTP mouse model of Parkinson's disease. Front. Pharmacol. 13, 935784. https://doi.org/10.3389/fphar.2022.935784.
Parkhe, A., Parekh, P., Nalla, L.V., Sharma, N., Sharma, M., Gadepalli, A., Kate, A., Khairnar, A., 2020. Protective effect of alpha mangostin on rotenone induced toxicity in rat model of Parkinson's disease. Neurosci. Lett. 716, 134652. https://doi.org/10.1016/j.neulet.2019.134652.
Pinna, A., Costa, G., Serra, M., Contu, L., Morelli, M., 2021. Neuroinflammation and L-dopa-induced abnormal involuntary movements in 6-hydroxydopamine-lesioned rat model of Parkinson's disease are counteracted by combined administration of a 5-HT1A/1B receptor agonist and A2A receptor antagonist. Neuropharmacology 196, 108693. https://doi.org/10.1016/j.neuropharm.2021.108693.
Pisanu, A., Lecca, D., Mulas, G., Wardas, J., Simbula, G., Spiga, S., Carta, A.R., 2014. Dynamic changes in pro- and anti-inflammatory cytokines in microglia after PPAR-γ agonist neuroprotective treatment in the MPTPp mouse model of progressive Parkinson's disease. Neurobiol. Dis. 71, 280–291. https://doi.org/10.1016/j.nbd.2014.08.011.
Pupyshev, A.B., Tikhonova, M.A., Akopyan, A.A., Tenditnik, M.V., Dubrovina, N.I., Korolenko, T.A., 2019. Therapeutic activation of autophagy by combined treatment with rapamycin and trehalose in a mouse MPTP-induced model of Parkinson's disease. Pharmacol. Biochem. Behav. 177, 1–11. https://doi.org/10.1016/j.pbb.2018.12.005.
Qu, Y., Wang, L., Mao, Y., 2022. Gallic acid attenuates cerebral ischemia/re-perfusion-induced blood–brain barrier injury by modifying polarization of microglia. J. Immunotoxicol. 19, 17–26. https://doi.org/10.1080/1547691X.2022.2043494.
Rabaneda-Lombarte, N., Serratosa, J., Bové, J., Vila, M., Saura, J., Solà, C., 2021. The CD200R1 microglial inhibitory receptor as a therapeutic target in the MPTP model of Parkinson's disease. J. Neuroinflammation 18, 88. https://doi.org/10.1186/s12974-021-02132-z.
Ramos-Molina, A.R., Tejeda-Martínez, A.R., Viveros-Paredes, J.M., Chaparro-Huerta, V., Urmeneta-Ortíz, M.F., Ramírez-Jirano, L.J., Flores-Soto, M.E., 2023. Beta-caryophyllene inhibits the permeability of the blood–brain barrier in MPTP-induced parkinsonism. Neurología. https://doi.org/10.1016/j.nrl.2022.11.004. S0213485323000324.
Rodrigues, R.W.P., Gomide, V.C., Chadi, G., 2001. Astroglial and microglial reaction after a partial nigrostriatal degeneration induced by the striatal injection of different doses of 6-Hydroxydopamine. Int. J. Neurosci. 109, 91–126. https://doi.org/10.3109/00207450108986528.
Rousselet, E., Callebert, J., Parain, K., Joubert, C., Hunot, S., Hartmann, A., Jacque, C., Perez-Diaz, F., Cohen-Salmon, C., Launay, J.-M., Hirsch, E.C., 2002. Role of TNF-α receptors in mice intoxicated with the parkinsonian toxin MPTP. Exp. Neurol. 177, 183–192. https://doi.org/10.1006/exnr.2002.7960.
Roy, R., Paul, R., Bhattacharya, P., Borah, A., 2023. Combating dopaminergic neurodegeneration in Parkinson's disease through Nanovesicle technology. ACS Chem. Neurosci. 14, 2830–2848. https://doi.org/10.1021/acschemneuro.3c00070.
Santoro, M., Fadda, P., Klephan, K.J., Hull, C., Teismann, P., Platt, B., Riedel, G., 2023. Neurochemical, histological, and behavioral profiling of the acute, sub-acute, and chronic MPTP mouse model of Parkinson's disease. J. Neurochem. 164, 121–142. https://doi.org/10.1111/jnc.15699.
Schirinzi, T., Madeo, G., Martella, G., Maltese, M., Picconi, B., Calabresi, P., Pisani, A., 2016. Early synaptic dysfunction in Parkinson's disease: insights from animal models. Mov. Disord. 31, 802–813. https://doi.org/10.1002/mds.26620.
Serra, M., Di Maio, A., Bassareo, V., Nuzzo, T., Errico, F., Servillo, F., Capasso, M., Parekh, P., Li, Q., Thiolat, M.-L., Bezard, E., Calabresi, P., Sulzer, D., Carta, M., Morelli, M., Usiello, A., 2023. Perturbation of serine enantiomers homeostasis in the striatum of MPTP-lesioned monkeys and mice reflects the extent of dopaminergic midbrain degeneration. Neurobiol. Dis. 184, 106226. https://doi.org/10.1016/j.nbd.2023.106226.
Sriram, K., Matheson, J.M., Benkovic, S.A., Miller, D.B., Luster, M.I., O'Callaghan, J.P., 2002. Mice deficient in TNF receptors are protected against dopaminergic neurotoxicity: implications for Parkinson's disease. FASEB J. 16, 1474–1476. https://doi.org/10.1096/fj.02-0216fje.
Stefanova, N., 2022. Microglia in Parkinson's Disease. JPD 12, S105–S112. https://doi.org/10.3233/JPD-223237.
Subedi, L., Lee, S.E., Madiha, S., Gaire, B.P., Jin, M., Yumnam, S., Kim, S.Y., 2020. Phytochemicals against TNFα-mediated neuroinflammatory diseases. IJMS 21, 764. https://doi.org/10.3390/ijms21030764.
Tansey, M.G., Wallings, R.L., Houser, M.C., Herrick, M.K., Keating, C.E., Joers, V., 2022. Inflammation and immune dysfunction in Parkinson disease. Nat. Rev. Immunol. 22, 657–673. https://doi.org/10.1038/s41577-022-00684-6.
Tavares, G., Martins, M., Correia, J.S., Sardinha, V.M., Guerra-Gomes, S., Das Neves, S.P., Marques, F., Sousa, N., Oliveira, J.F., 2017. Employing an open-source tool to assess astrocyte tridimensional structure. Brain Struct. Funct. 222, 1989–1999. https://doi.org/10.1007/s00429-016-1316-8.
Torres-Ceja, B., Olsen, M.L., 2022. A closer look at astrocyte morphology: development, heterogeneity, and plasticity at astrocyte leaflets. Curr. Opin. Neurobiol. 74, 102550. https://doi.org/10.1016/j.conb.2022.102550.
Walker, D.G., Lue, L.-F., Serrano, G., Adler, C.H., Caviness, J.N., Sue, L.I., Beach, T.G., 2016. Altered expression patterns of inflammation-associated and trophic molecules in substantia Nigra and striatum brain samples from Parkinson's disease, incidental Lewy body disease and Normal control cases. Front. Neurosci. 9. https://doi.org/10.3389/fnins.2015.00507.
Wang, Q., Shin, E.-J., Nguyen, X.-K.T., Li, Q., Bach, J.-H., Bing, G., Kim, W.-K., Kim, H.-C., Hong, J.-S., 2012. Endogenous dynorphin protects against neurotoxin-elicited nigrostriatal dopaminergic neuron damage and motor deficits in mice. J. Neuroinflammation 9, 583. https://doi.org/10.1186/1742-2094-9-124.
Wang, T., Sun, Y., Dettmer, U., 2023. Astrocytes in Parkinson's disease: from role to possible intervention. Cells 12, 2336. https://doi.org/10.3390/cells12192336.
World Health Organization, 2023. Parkinson's disease. World Health (Organization). https://www.who.int/news-room/fact-sheets/detail/parkinson-disease.
Xiromerisiou, G., Marogianni, C., Lampropoulos, I.C., Dardiotis, E., Speletas, M., Ntavaroukas, P., Androutsopoulou, A., Kalala, F., Grigoriadis, N., Papoutsopoulou, S., 2022. Peripheral inflammatory markers TNF-α and CCL2 revisited: association with Parkinson's disease severity. IJMS 24, 264. https://doi.org/10.3390/ijms24010264.
Yarim, G.F., Kazak, F., Yarim, M., Sozmen, M., Genc, B., Ertekin, A., Gokceoglu, A., 2022. Apigenin alleviates neuroinflammation in a mouse model of Parkinson's disease. Int. J. Neurosci. 1–10. https://doi.org/10.1080/00207454.2022.2089136.
Yin, R., Xue, J., Tan, Y., Fang, C., Hu, C., Yang, Q., Mei, X., Qi, D., 2021. The positive role and mechanism of herbal medicine in Parkinson's disease. Oxidative Med. Cell. Longev. 2021, 1–23. https://doi.org/10.1155/2021/9923331.
Yu, X., Yao, J.-Y., He, J., Tian, J.-W., 2015. Protection of MPTP-induced neuroinflammation and neurodegeneration by rotigotine-loaded microspheres. Life Sci. 124, 136–143. https://doi.org/10.1016/j.lfs.2015.01.014.
Zahedipour, F., Hosseini, S., Henney, N., Barreto, G., Sahebkar, A., 2022. Phytochemicals as inhibitors of tumor necrosis factor alpha and neuroinflammatory responses in neurodegenerative diseases. Neural Regen. Res. 17, 1675. https://doi.org/10.4103/1673-5374.332128.
Zhou, X., Lu, J., Wei, K., Wei, J., Tian, P., Yue, M., Wang, Y., Hong, D., Li, F., Wang, B., Chen, T., Fang, X., 2021. Neuroprotective effect of ceftriaxone on MPTP-induced Parkinson's disease mouse model by regulating inflammation and intestinal microbiota. Oxidative Med. Cell. Longev. 2021, 1–15. https://doi.org/10.1155/2021/9424582.